HAL
open science

1-deoxysphingolipids bind to COUP-TF to modulate lymphatic and cardiac cell development

Ting Wang, Zheng Wang, Lauriane de Fabritus, Jinglian Tao, Essa Saied, Ho-Joon Lee, Bulat Ramazanov, Benjamin Jackson, Daniel Burkhardt, Mikhail Parker, et al.

To cite this version:

Ting Wang, Zheng Wang, Lauriane de Fabritus, Jinglian Tao, Essa Saied, et al.. 1-deoxysphingolipids bind to COUP-TF to modulate lymphatic and cardiac cell development. Developmental Cell, 2021, 56 (22), pp.3128-3145.e15. 10.1016/j.devcel.2021.10.018 . hal-03566022

HAL Id: hal-03566022

https://amu.hal.science/hal-03566022v1

Submitted on 16 May 2022

HAL is a multi-disciplinary open access archive for the deposit and dissemination of scientific research documents, whether they are published or not. The documents may come from teaching and research institutions in France or abroad, or from public or private research centers.

L'archive ouverte pluridisciplinaire **HAL**, est destinée au dépôt et à la diffusion de documents scientifiques de niveau recherche, publiés ou non, émanant des établissements d'enseignement et de recherche français ou étrangers, des laboratoires publics ou privés.

1-deoxysphingolipids bind to COUP-TF to modulate lymphatic and cardiac cell development

Graphical abstract

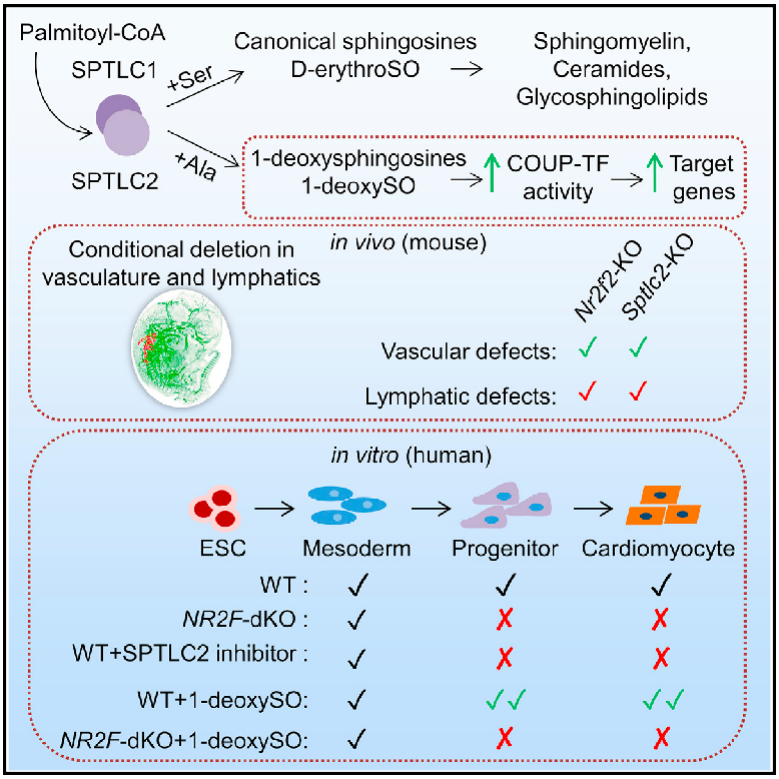

Highlights

- 1-deoxyphingosines bind and modulate NR2F1 and NR2F2 transcriptional activity
- Genetic deletion of *Sptlc2* phenocopies *Nr2f2* deficiency in lymphatic development
- Inhibition of sphingolipid synthesis impairs human cardiomyocyte differentiation
- 1-deoxysphingosine supplementation promotes human cardiomyocyte maturation

Authors

Ting Wang, Zheng Wang, Lauriane de Fabritus, ..., Susan M. Kaech, Natalia B. Ivanova, Fabio R. Santori

Correspondence

skaech@salk.edu (S.M.K.), natalia.ivanova@uga.edu (N.B.I.), fabio.santori@yale.edu (F.R.S.)

In brief

Wang et al. identify 1-deoxysphingosines as modulators of COUP-TF activity. Inhibition of sphingolipid biosynthesis mimics COUP-TF knockout phenotypes in lymphatic development and in human ESC-derived cardiomyocytes, whereas elevated levels of 1-deoxysphingosines enhance cardiomyocyte differentiation. Thus, sphingolipids could be physiological ligands for COUP-TFs and could play a critical role in development.

1-deoxysphingolipids bind to COUP-TF to modulate lymphatic and cardiac cell development

Ting Wang,[1,2,16] Zheng Wang,[3,4,16] Lauriane de Fabritus,[5,16] Jinglian Tao,[2,6,16] Essa M. Saied,[7,8] Ho-Joon Lee,[9,10] Bulat R. Ramazanov,[11] Benjamin Jackson,[6] Daniel Burkhardt,[9] Mikhail Parker,[6] Anne S. Gleinich,[12] Zhirui Wang,[12] Dong Eun Seo,[6] Ting Zhou,[1] Shihao Xu,[13] Irina Alecu,[14] Parastoo Azadi,[12] Christoph Arenz,[7] Thorsten Hornemann,[15] Smita Krishnaswamy,[9] Serge A. van de Pavert,[5] Susan M. Kaech,[13,*] Natalia B. Ivanova,[6,*] and Fabio R. Santori[1,17,*]
[1]Department of Immunobiology, Yale University, New Haven, CT 06520, USA
[2]Department of Hematology, Tianjin Medical University General Hospital, Tianjin 300052, China
[3]Department of Genetics and Cell Biology, Basic Medical College, Qingdao University, Qingdao, Shandong 266071, China
[4]Department of Reproductive Medicine, the Affiliated Hospital of Qingdao University, Qingdao, Shandong 266000, China
[5]Aix-Marseille Universite, CNRS, INSERM, Centre d'Immunologie de Marseille-Luminy (CIML), 13288 Marseille Cedex 9, France
[6]Center for Molecular Medicine, Department of Genetics, University of Georgia, Athens, GA 30602, USA
[7]Institut fu€r Chemie, Humboldt Universita€t zu Berlin, Berlin 12489, Germany
[8]Chemistry Department, Faculty of Science, Suez Canal University, Ismailia 41522, Egypt
[9]Department of Genetics, Yale University, New Haven, CT 06520, USA
[10]Center for Genome Analysis, Yale University, New Haven, CT 06510, USA
[11]Department of Cell Biology, Yale University, New Haven, CT 06520, USA
[12]Complex Carbohydrate Research Center, University of Georgia, Athens, GA 30602, USA
[13]NOMIS Center for Immunobiology and Microbial Pathogenesis, the Salk Institute for Biological Studies, La Jolla, CA 92037, USA
[14]Neural Regeneration Laboratory, Department of Biochemistry, Microbiology, and Immunology, University of Ottawa, Ottawa K1H 8M5, Canada
[15]Institute of Clinical Chemistry, University and University Hospital of Zurich, Zurich 8091, Switzerland
[16]These authors contributed equally
[17]Lead contact
*Correspondence: skaech@salk.edu (S.M.K.), natalia.ivanova@uga.edu (N.B.I.), fabio.santori@yale.edu (F.R.S.)
https://doi.org/10.1016/j.devcel.2021.10.018

SUMMARY

Identification of physiological modulators of nuclear hormone receptor (NHR) activity is paramount for understanding the link between metabolism and transcriptional networks that orchestrate development and cellular physiology. Using libraries of metabolic enzymes alongside their substrates and products, we identify 1-deoxysphingosines as modulators of the activity of NR2F1 and 2 (COUP-TFs), which are orphan NHRs that are critical for development of the nervous system, heart, veins, and lymphatic vessels. We show that these non-canonical alanine-based sphingolipids bind to the NR2F1/2 ligand-binding domains (LBDs) and modulate their transcriptional activity in cell-based assays at physiological concentrations. Furthermore, inhibition of sphingolipid biosynthesis phenocopies NR2F1/2 deficiency in endothelium and cardiomyocytes, and increases in 1-deoxysphingosine levels activate NR2F1/2-dependent differenti- ation programs. Our findings suggest that 1-deoxysphingosines are physiological regulators of NR2F1/2-mediated transcription.

INTRODUCTION

Nuclear hormone receptors (NHRs) are transcription factors regulated by small molecules, such as endogenous metabolites, hormones, or diet-derived compounds including vitamins and fatty acids (Tao et al., 2020). These ligands can either bind the ligand-binding pocket (orthosteric ligands) or to alternative sites in the ligand-binding domain (LBD) of the NHR (allosteric ligands) (van Westen et al., 2014). Most natural NHR ligands are orthosteric, but 27-hydroxycholesterol was recently identified as a natural allosteric ligand for ERb (Starkey et al., 2018). There are 48 NHRs in the human genome, including 36 non-classic receptors and 12 classic NHRs for vitamins A, D, and steroid hormones. There are 19 orphan NHRs, where no natural ligand is known (Tao et al., 2020). The identification of these ligands is central to understanding the relationship between metabolic activity and gene transcription.

The NR2F family is comprised of three members: NR2F1/COUP-TFI, NR2F2/COUP-TFII, and NR2F6/EAR2 (Jonk et al., 1994). NR2F1/2 have evolutionarily conserved roles in neurogenesis. NR2F1/2 homologs are expressed in the neural lineage of *Hydra*, a cnidarian (Gauchat et al., 2004), and in *C. elegans* the

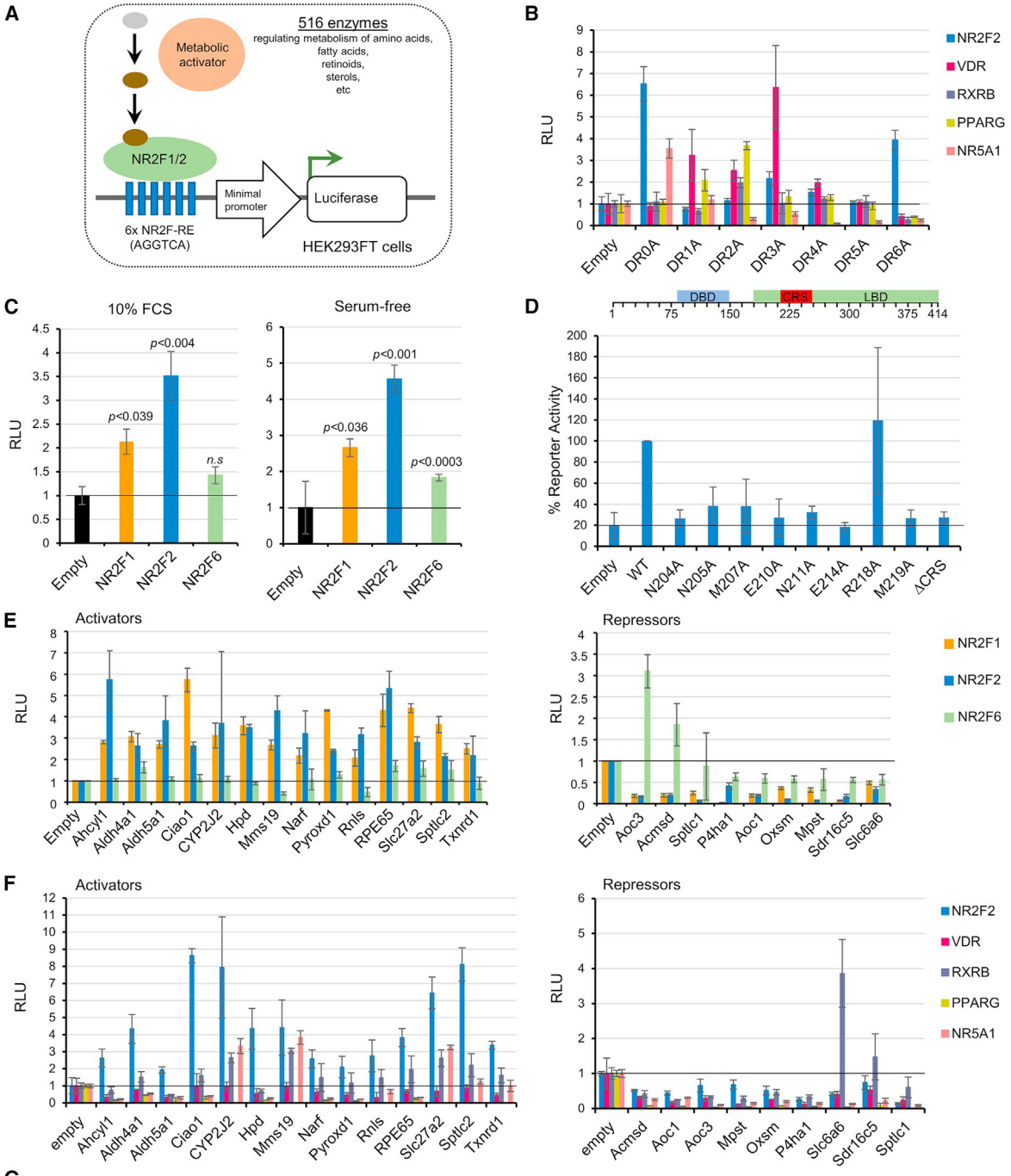

G

Pathway	Enzymes
Iron-sulfur cluster biosynthesis	MMS19, CIAO1, NARF
Retinol and fatty acid metabolism	RPE65
Fatty acid metabolism	SLC27A2, CYP2J2
Amino acid metabolism	AHCYL1, ALDH4A1, ALDH5A1 (Ala, Asp, Glu), HPD (Phe, Tyr), TXNRD1 (multiple pathways)
Sphingolipid metabolism	SPTLC2
Unknown	PYROXD1, RNLS

(legend on next page)

NR2F1/2 homolog unc-55 is required for the proper development of interneuron networks (Petersen et al., 2011; Shan and Walthall, 2008). In *Drosophila melanogaster* the NR2F1/2 homolog Svp regulates the differentiation of photoreceptor cells (Mlodzik et al., 1990) and neural lineages derived from type I and II neuroblasts (Kanai et al., 2005; Maurange et al., 2008; Mettler et al., 2006) as well as the development of valve-like ostiae in the fly heart (Molina and Cripps, 2001; Ponzielli et al., 2002). Vertebrates have two homologous NR2F receptors, NR2F1 and NR2F2, with partially redundant functions. Deletion of all four NR2F1/2 alleles in mice causes major eye defects such as coloboma and microphthalmia (Tang et al., 2010). NR2F1 and NR2F2 also possess non-redundant functions. NR2F1 regulates the development of oligodendrocytes (Yamaguchi et al., 2004), formation of glossopharyngeal cranial nerves IX, and axon guidance and arborization in the peripheral nervous system (Qiu et al., 1997). Haploinsufficiency of NR2F1 causes of Bosch-Boonstra-Schaaf optic atrophy syndrome in humans (Bosch et al., 2014). In contrast, NR2F2 is required for cardiac development in both mice (Pereira et al., 1999) and humans (Al Turki et al., 2014), the formation of GABAergic interneurons in the mouse brain (Kanatani et al., 2015), and the development of both venous (You et al., 2005) and lymphatic endothelia in mice (Lin et al., 2010; Srinivasan et al., 2007). The third member of the NR2F family, NR2F6, plays a role in the differentiation of pro-inflammatory $CD4^+$ Th17 cells (Hermann-Kleiter et al., 2008). Despite their ubiquity during development, the metabolic pathways that regulate the activity of NR2F NHRs are unknown.

Biochemical approaches and candidate metabolite screening methods have been used to identify the ligands of the orphan NHRs RXR (Heyman et al., 1992; Levin et al., 1992), LXR (Janowski et al., 1996), and FXR (Makishima et al., 1999; Parks et al., 1999). However, these approaches have not succeeded in all orphan NHRs. Here, we develop a strategy, which combines enzyme overexpression and metabolite screening, to identify 1-deoxysphingosines as modulators of NR2F1/2 activity. Our study suggests a physiological role for 1-deoxysphingosines as modulators of NR2F1/2-mediated transcription.

RESULTS

Metabolic enzyme overexpression screening identifies pathways that modulate NR2F1/2 transcriptional activity

We reasoned that, if endogenous metabolites regulate NR2F1/2 proteins, then overexpression of enzymes within the metabolic pathways responsible for ligand synthesis would modulate NR2F1/2 transcriptional activity and such pathways could be identified using an appropriate reporter assay (Figure 1A). The LBDs of NR2F1 and NR2F2 are 95% identical (Jonk et al., 1994; Qiu et al., 1994) (Figure S1A) and likely recognize the same ligand. Thus, modulation of reporter activity would be pro- moted by the same enzymes for both receptors. In contrast, the LBD of NR2F6 exhibits significantly lower amino acid identity to NR2F1/2 (~60%) (Figure S1A), suggesting that NR2F6 may bind a different ligand and serve as specificity control. We utilized wild-type full-length NR2F1/2/6 receptors to optimize the specificity and sensitivity of our luciferase reporter. We screened a set of DNA sequences composed of six conserved direct repeats (DRs) of the NR2F response element AGGTCA separated by spacers of zero (6xDR0A) to six (6xDR6A) adenines (Montemayor et al., 2010; Pipao´ n et al., 1999). A peak of NR2F1/2 reporter activity was observed with the 6xDR0A reporter when compared with the baseline empty vector control (Figure 1B). Previous studies suggested that NR2F1/2 could interact with other NHRs, such as RXRs, VDR, or PPARs, leading to activation or repression of their transcriptional activity (Tsai and Tsai, 1997). To evaluate the potential confounding effect from other NHRs in our reporter assays, we transfected HEK-293FT cells with native full-length constructs of VDR, RXRB, PPARG, and NR5A1 and found that, except for NR5A1, unrelated receptors did not increase the activity of the 6xDR0A reporter (Figure 1B). RXRB and VDR required reporters with different spacers (Figure 1B) plus addition of their respective ligands, 9-*cis*-retinoic acid and vitamin D, to induce their transcriptional activity (Figure S1B). These results confirmed that the activity of the 6xDR0A reporter in HEK-293FT cells was specific to NR2F1/2.

Transfection of native full-length *Nr2f1* or *Nr2f2* cDNAs increased reporter activity in both serum-containing and serum-free media (Figure 1C), suggesting that HEK-293FT cells expressed the metabolic pathways required for production of NR2F1/2 ligand. NR2F1/2 activity was dependent on coactivator recruitment by the NR2F2 LBD. Indeed, the activity of the full-length NR2F2 was inhibited by point mutations within the LBD as well as deletion of the coactivator recognition site (CRS) (Figure 1D). Furthermore, the activity of the NR2F1(LBD)-GAL4(DBD) fusion protein was inhibited by 4-methoxy-1-naphthol, a specific NR2F1/2 inhibitor that binds to the CRS (Le Gue´ vel et al., 2017) (Figure S1C). Taken together, these results indicate that reporter activity of NR2F1/2 in HEK-293FT cells is specific and coactivator dependent.

To identify metabolic pathways that regulate NR2F1/2 activity, we selected 516 cDNAs of enzymes that cover most reactions driving the metabolism of common biosynthetic molecules in mammalian cells, such as amino acids, fatty acids, retinoids, sterols, etc. These enzymes were tested individually in HEK-293FT

Figure 1. Enzyme overexpression screening identifies modulators of NR2F1/2 transcriptional activity

(A) Reporter system used in the overexpression screen.

(B) Reporter constructs with DR0A spacing are specific for NR2F2. Cells were grown in medium with 10% FCS with no added ligand. Values: relative light units (RLU). Error bars are standard deviation.

(C) Reporter activity is induced by native full-length NR2F1, NR2F2, and NR2F6 receptors in both FCS-containing and serum-free medium. Error bars are standard deviation and p-values were defined using two tailed Student's t test.

(D) NR2F2 activity is abolished by mutations in the coactivator recognition site (CRS). Error bars are standard deviation.

(E) Metabolic enzymes modulate the activity of native full-length NR2F1/2 receptors. Activators (left) upregulated reporter activity by >2-fold. Repressors (right) downregulated reporter activity by >2-fold. Error bars are standard deviation.

(F) Activating enzymes are specific for native full-length NR2F1/2. Error bars are standard deviation.

(G) Summary of pathways modulating NR2F1/2 activity.

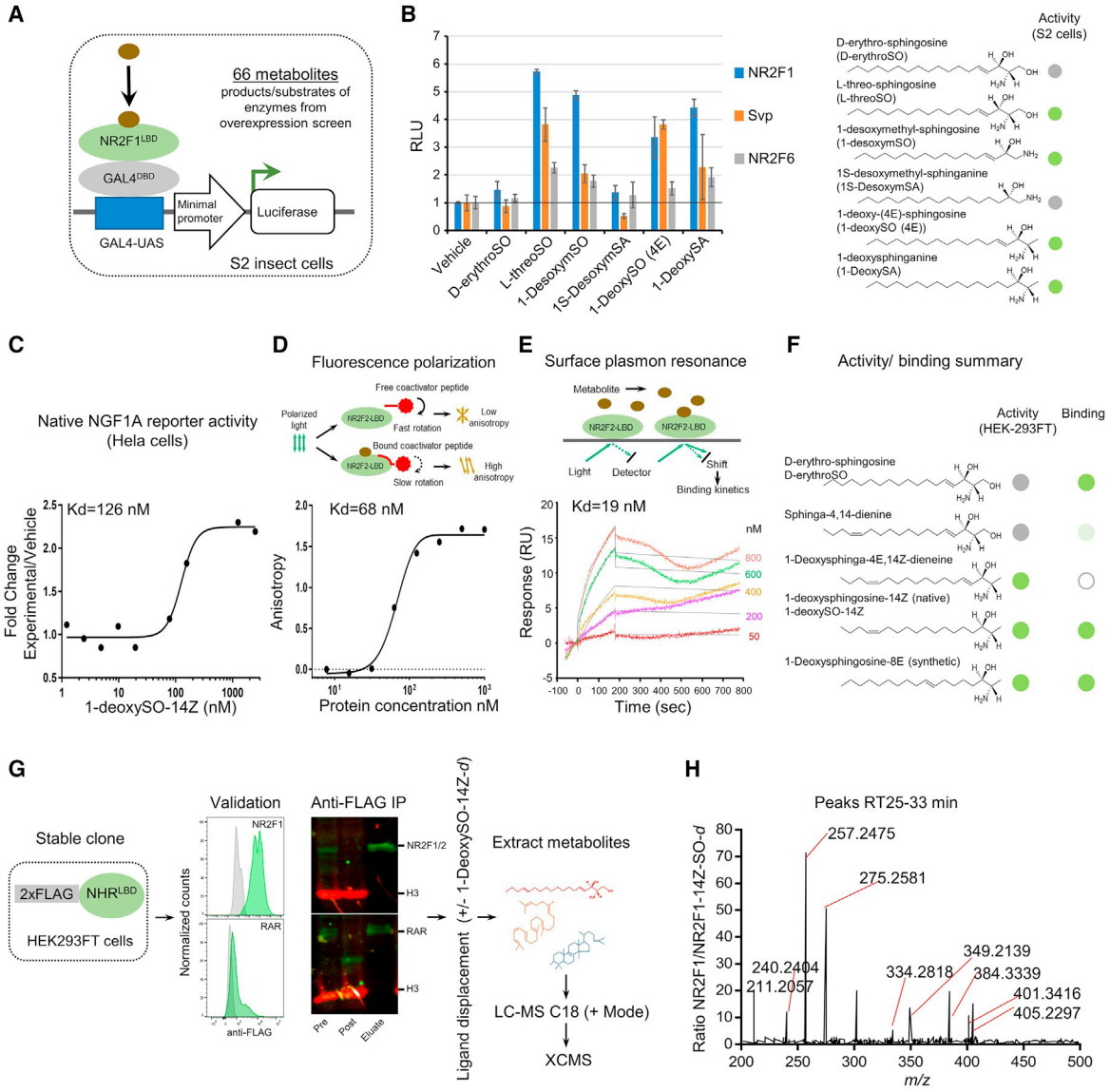

I

Putative sphingosines RT25-33 min

Mode	mzmed	Adduct	ppm	rtmed	Name	maxint	p-value	Fold F1/14Z
C18 +	334.2818	[M+Na]+	32	32.7086	(4E,8E,9Me-d19:2)sphingosine	52738	0.0234	5.3224
C18 +	257.2475	275-[M+H-H2O]+	25	32.5992	275-[-H2O]	868690	0.0116	71.3576
C18 +	275.2581	[M+NH4]+	40	32.5992	D-erythro-Sphingosine C-15	133524	0.0095	50.6178
C18 +	240.2404	[M+H-H2O]+	32	32.5992	D-erythro-Sphingosine C-15	71004	0.0169	12.0178

J

Specificity and enrichment of 1-deoxySO-14Z-*d* in NR2F-LBD

							Specificity		Enrichment	
Mode	Ion	Adduct	ppm	rtmed	Name	maxint	Fold Change 14ZNR2F/14ZRAR	p-value	Fold Change 14ZNR2F/NR2F	p-value
C18 +	286.2824	[M+H]+	28	35.26020	1-deoxySO-14Z-*d*	53032	12.2983	0.002565	29.757651	0.001747
C18 +	303.2896	[M+NH4]+	36	35.23375	1-deoxySO-14Z-*d*	35114	16.15044	0.002451	19.0693706	0.001915
C18 +	268.2681	[M+H-H2O]+	15	35.12772	1-deoxySO-14Z-*d*	34366	1.42408	0.271658	22.0502266	0.04892

Figure 2. Non-canonical alanine-based sphingolipids are NR2F1/2 ligands

(A) Insect-cell-based system for metabolite screening.

(B) Sphingolipids promote NR2F reporter activity in insect cells. Circles: active (green), inactive (gray), and not tested (white). Error bars are standard deviation.

(C) 1-deoxySO-14Z promotes transcriptional activity of NR2F2 in cells transfected with native promoter-based NGF1A reporter.

(D) 1-deoxySO-14Z binds recombinant NR2F2 LBD in FPA.

(legend continued on next page)

cells by co-transfection with the native full-length NR2F1/2 receptor and 6xDR0A reporter (Figure 1A). We identified 14 metabolic enzymes that upregulated the transcriptional activity of both NR2F1 and NR2F2 by more than 2-fold compared with empty vector control, without increasing NR2F6 reporter activity. In addition, 9 enzymes downregulated transcriptional activity of NR2F1 and NR2F2 by more than 2-fold, without decreasing NR2F6 reporter activity (Figure 1E). The effect of each enzyme on NR2F2 reporter activity was confirmed using a luciferase reporter driven by the NGF1A promoter, a native NR2F2 target (Pipao´ n et al., 1999) (Figure S1F). Three enzymes in the NR2F1/2 set—AOC3, RNLS, and MMS19—had the opposite effect on NR2F6 reporter activity suggesting that ligands for NR2F1/2 and NR2F6 may be products of different branches of the same metabolic pathway. When re-tested against a panel of several unrelated full-length NHRs such as RXRB, VDR, PPARG, or NR5A1, most NR2F2 activators were specific and did not increase the reporter activity of these receptors (Figure 1F). Only three enzymes—CYP2J2, MMS19, and SLC27A2—increased reporter activity of NR5A1 on the 6xDR0A reporter (Figures 1B and 1F). In contrast, none of the repressors identified in the screen were specific for NR2F1/2 (Figure 1F).

Notably, sphingosines bind and antagonize NR5A1, but this repression is dependent on ceramide degradation by ceramidases, which are interacting partners of NR5A1 (Urs et al., 2006), rather than the *de novo* synthesis of sphingo- sine. Several enzymes in the ceramide synthesis/degradation pathways including ACER1, ASAH2B, CERS2, and CERK were tested but had no significant effect on NR2F1/2 re- porter activity in our screen (data not shown). Likewise, overexpression of SPTLC2, the enzyme regulating sphingolipid biosynthesis, did not affect NR5A1 reporter activity (Fig- ure 1F). Thus, the activities of NR2F1/2 and NR5A1 may be modulated by different pools of sphingosines: NR2F1/2 by sphingosine biosynthesis while NR5A1 by sphingosine catabolism.

When assigned to known metabolic pathways (Kanehisa et al., 2017; Stehling et al., 2013), the enzymes identified in our screen fell into four pathways: iron-sulfur cluster biosynthesis, amino acid metabolism, retinol and fatty acid metabolism, and sphingolipid biosynthesis (Figure 1G). Several enzymes that upregulated NR2F1/2 activity also upregulated the synthesis of D-erythro-sphingosine (Figure S1G). Previous reports suggested that at high concentrations, all-*trans* retinoic acid is a weak agonist of NR2F2 (Kruse et al., 2008). Our screens tested 29 enzymes and retinoids in the retinoic acid pathway, but none affected NR2F1/2 transcriptional activity in our system (Figures S1H and S1I).

Taken together, our screen identified four metabolic pathways that modulated NR2F1/2 activity: iron-sulfur cluster biosynthesis, sphingolipid biosynthesis, and fatty acid/amino acid metabolism.

Non-canonical alanine-based sphingolipids are NR2F1/2 ligands

Next, we tested 66 commercially available substrates and products of enzymes in the metabolic pathways that modulated NR2F1/2 activity (see STAR Methods). We utilized a GAL4-UAS-driven luciferase reporter to monitor the activity of the NR2F1(LBD)-GAL4 (DBD) and fly NR2F1/2 homolog Svp(LBD)-GAL4(DBD) fusion proteins in *Drosophila melanogaster* S2 cells in response to these metabolites (Figure 2A). This reporter system produces low background noise and is ideal for the detection of weak activity (Santori et al., 2015). While none of the metabolites in the iron-sulfur cluster biosynthesis, fatty acid, or amino acid metabolism pathways were active, transcrip- tional activity of the NR2F1-GAL4 fusion protein was promoted by several non-canonical sphingolipids, including 1-deoxysphingosine (1-deoxySO), 1-deoxysphinganine (1-deoxySA), and 1-deoxymethylsphingosine (1-deoxymSO), all of which are products of SPTLC1/2 enzymes (Figure 2B).

To determine structure-activity relationship, we tested variants of active 1-deoxysphingolipids (Saied and Arenz, 2021; Saied et al., 2018). 1-deoxySO with D14 double bond in the sphingoid base (Steiner et al., 2016) promoted transcriptional activity of native full-length NR2F2 in HeLa cells with a Kd = 126 nM (Figure 2C). Under physiological conditions, sphingoli- pids are primarily derived from serine, with a minor fraction made using glycine or alanine. Strikingly, neither serine-based (D-erythro-sphingosine) nor glycine-based (1-desoxymethylSO) sphingolipids had activity in our insect-cell-based metabolite screen (Figure 2B). The desaturation at positions D8 or D14 of the lipid tail of 1-deoxySO enhanced NR2F2 transcriptional activity (Figure S2A), suggesting that the absence of a C1 hydroxyl group and the presence of D4 and D14 unsaturation were key structural features of NR2F1/2 ligands.

Next, we tested the binding of sphingolipids to recombinant NR2F1 and 2-LBD *in vitro*. We found that 1-deoxySO-14Z bound to NR2F2-LBD with an affinity of 68 nM by fluorescence polarization assays (FPAs) (Figures 2D and S2B) and 19 nM by surface plasmon resonance (SPR) (Figure 2E). Thus, for 1-deoxySO-14Z, FPA and SPR measurements suggest an affinity in the range of 10–100 nM. In contrast, a canonical serine-based sphingosine (D-erythroSO) that had no detectable activity in our native reporter assay (Figure S2C) bound to NR2F1/2 LBD with an affinity of 59 nM determined by SPR (Figure S2D) and Kd > 300 nM by FPA (Figure S2B). The SPR measures direct interaction of metabolite and protein, whereas FPA measures the ability of a compound to promote coactivator peptide recruitment, which is a surrogate for agonist activity. Thus, our data suggest that both D-erythroSO and 1-deoxySO-14Z bind NR2F1/2 LBD at nanomolar concentrations, but of the two types of sphingosines 1-deoxysphingosines are better agonists. Other sphingolipids such as sphinga-4,14-dienine (sphinga-4,14) stabilized NR2F2 LBD in thermal shift assay (Figure S2E) but had low affinity for

(E) 1-deoxySO-14Z binds recombinant NR2F2 LBD by SPR.
(F) Summary of structure-activity relationships of 1-deoxysphingolipids in mammalian cells. Circles: active (green), inactive (gray), and white (not tested).
(G) Metabolite pull-down experimental scheme.
(H) Metabolites displaced from NR2F1 LBD by 1-deoxySO-14Z-*d*.
(I) Summary of m/z ions (H) identified in the 25–33 min retention time interval.
(J) Specificity and enrichment of 1-deoxySO-14Z-*d* in NR2F1 LBD compared with RAR LBD and NR2F1 LBD vehicle.

NR2F2 LBD (>300 nM by FP and >700 nM by SPR). We found that active sphingolipids bound both NR2F1 and NR2F2 LBDs, therefore supporting our hypothesis that these receptors are modulated by the same metabolites (Figure S2B). Our measurements suggest that the Kd of 1-deoxysphingosines for NR2F1/2 was well below their plasma concentrations of 300 nM (Mwinyi et al., 2017; Othman et al., 2015). Thus, 1-deoxysphingosines could potentially modulate NR2F1/2 activity in physiological settings. The binding and biological activities of the different sphingolipids are summarized in Figures 2B, 2F, and S2A.

If 1-deoxysphingosines bind to NR2F1/2 produced in mammalian cells, then synthetic ligands would not only bind to NR2F1/2 LBD but would also displace endogenous metabolites bound to the receptor. Therefore, we tested whether deuterated 1-deoxySO-14Z (1-deoxySO-14Z-*d*) displaced endogenous metabolites bound to NR2F1 LBD in mammalian cells (Figure 2G). FLAG-tagged NR2F1 LBD was expressed and purified from HEK-293FT cells side by side with the LBD of retinoic acid receptor alpha (RARA), which was used as a control. The purified LBDs were incubated with either a vehicle or 1-deoxySO-14Z-*d*, and displaced metabolites were isolated and identified by LC-MS. Several NR2F1-bound metabolites displaced by 1-deoxySO-14Z-*d* matched exact masses corresponding to those of sphingosines (Figures 2H and 2I). Furthermore, 1-deoxySO-14Z-*d* was enriched in the NR2F1 but not in the RARA samples (Figure 2J), suggesting that 1-deoxySO- 14Z specifically bound to NR2F1 LBD.

Notably, while metabolites with exact masses of retinoic acid, a high-affinity ligand for RARs (Giguere et al., 1987; Petkovich et al., 1987), were found in the RARA preparations, no such metabolites were detected in the NR2F1 samples (see STAR Methods). Indeed, retinoic acid is a low-affinity ligand for NR2F1/2 with a Kd = 26 mM (Kruse et al., 2008). This affinity is magnitudes below the 500 nM retinoic acid present in our medium and is too weak to be detected by our system.

1-deoxysphingosines could be either produced by cells themselves (autocrine route) or taken up from the medium (hormonal route). Sphingolipids, phospholipids, and glycerolipids are all synthesized from fatty acids (Figure S2F). Thus, if autocrine 1-deoxySO production is a significant source of NR2F1/2 ligand, NR2F1/2 transcriptional activity should be attenuated by the deletion of fatty acid synthase (FASN), the rate-limiting enzyme of fatty acid biosynthesis. In contrast, NR2F1/2 transcriptional activity should be increased by the deletion of enzymes, which decrease fatty acid availability such as PCYT1A and PCYT1B, which convert fatty acids to phosphatidylcholine (Walker et al., 2011). PCYT1A is normally expressed in HEK293FT cells, while PCYT1B is not and serves as a control. Loss of FASN significantly reduced the transcriptional activity of native full-length NR2F1/2 (Figure S2F), while deletion of PCYT1A increased NR2F2 and NR2F6 transcriptional activity (Figure S2F). The possible association of metabolic pathways identified in our study with sphingolipid biosynthesis are summarized in Figure S2G.

To estimate intracellular concentrations of canonical and non-canonical sphingolipids in NR2F2-expressing cells, we isolated cytosolic and nuclear fractions prepared from the telomerase-immortalized human microvascular endothelium (TIME) cells (Figure S2H). TIME cells contained 0.05 pmole of 1-deoxysphingosine/10^6 cells, and more than half was allocated to the nuclear fraction (Figure S2I). These amounts correspond to 50 nM concentration, which is around the Kd measured by *in vitro* binding assays. 1-deoxysphingosine can also be imported from the media. To test this route, TIME cells were incubated with 1-deoxySO fluorescently labeled with a nitrobenzoxadiazole group (NBD) and analyzed by confocal microscopy. Most NBD fluorescence was detected in the cytoplasm, but up to 20% of total fluorescence was observed in the nucleus (Figures S2J and S2K).

Phenotypes of *Sptlc2*$^{f/f}$ *Prox1*$^{Cre\text{-}ERT2/+}$ and *Sptlc2*$^{f/f}$ *Cdh5*$^{Cre\text{-}ERT2/+}$ embryos correlate to those of *Nr2f2* deficient animals

We hypothesized that if 1-deoxysphingosines are natural NR2F1/2 ligands, deletion of serine palmitoyltransferase (*Sptlc2*), which is the rate-limiting enzyme of sphingolipid biosynthesis, should correlate with *Nr2f1/2* gene deficiency *in vivo*. We examined the venous and lymphatic endothelium, as well as the heart, where *Nr2f2* gene function has previously been studied (Lin et al., 2010; Pereira et al., 1999; Srinivasan et al., 2007, 2010; You et al., 2005). Importantly, sphingolipids and 1-deoxysphingolipids are present in HDL and LDL (Hornemann et al., 2009), and genetic deletion of *Sptlc2* in both the liver and the heart has no effect on organ function in young animals (Lee et al., 2012a; Li et al., 2009). Thus, we expected that conditional *Sptlc2* deficiency could be partially rescued by HDL- and LDL-derived sphingolipids present in the fetal circulation, resulting in a phenotype that is milder than that observed in *Nr2f2*-defi- cient animals.

We intercrossed mice with a conditional *Sptlc*$^{f/f}$ allele (*Sptlc2* $^{tm2.1Jia}$) (Li et al., 2009) and the BAC transgenic mice carrying the tamoxifen (TM)-inducible Cre recombinase integrated into the *Prox1* locus (*Prox1*$^{Cre\text{-}ERT2}$) for deletion of *Sptlc2* in lymphatic vessels, vascular endothelial precursors, heart, and liver (Bazigou et al., 2011). We also intercrossed *Sptlc*$^{f/f}$ mice with *Cdh5*^{CreERT2} mice for deletion in endothelial cells (Wang et al., 2010). Time-mated pregnant females were injected with TM at E10.5. Embryos were collected at E13.5 and E15.5 and stained and analyzed as whole-mount by light-sheet microscopy (Figure 3A). Deletion of floxed *Sptlc2* allele was efficient, reaching 90% when measured in sorted PROX1+ cells and 60% when measured in whole heart, which is rich in PROX1+ cells (Figure 3B).

Deletion of *Nr2f2* in endothelial cells affects angiogenesis and venous blood vessel development (Pereira et al., 1999; You et al., 2005). Accordingly, we found reduced vascularization when *Sptlc2* was deleted in endothelial cells of *Sptlc2*^{Cdh5CreERT2} embryos. We observed this to a lesser degree in *Sptlc*^{Prox1CreERT2} embryos (Figure 3C). However, we did not observe gross abnormalities in the heart myocardium of *Prox1*$^{Cre\text{-}ERT2}$ and *Cdh5*$^{Cre\text{-}ERT2}$ models such as those reported in full *Nr2f2* knockouts at earlier stages of development (Pereira et al., 1999). *Sptlc2* deficiency in either the *Prox1*$^{Cre\text{-}ERT2}$ or *Cdh5*$^{Cre\text{-}ERT2}$ models failed to produce viable progeny for studies in adult animals.

We analyzed the lymphatic endothelium of TM-treated *Sptlc2*$^{f/f}$ *Prox-1*$^{Cre\text{-}ERT2}$ and *Sptlc2*$^{f/f}$ *Cdh5*^{CreERT2} embryos. Deletion of *Nr2f2* in lymphatic endothelium results in fetal edema, blood-filled lymphatics, defects in the development of lymphatic sacs, and dilated skin lymphatic vessels (Lin et al., 2010; Srinivasan

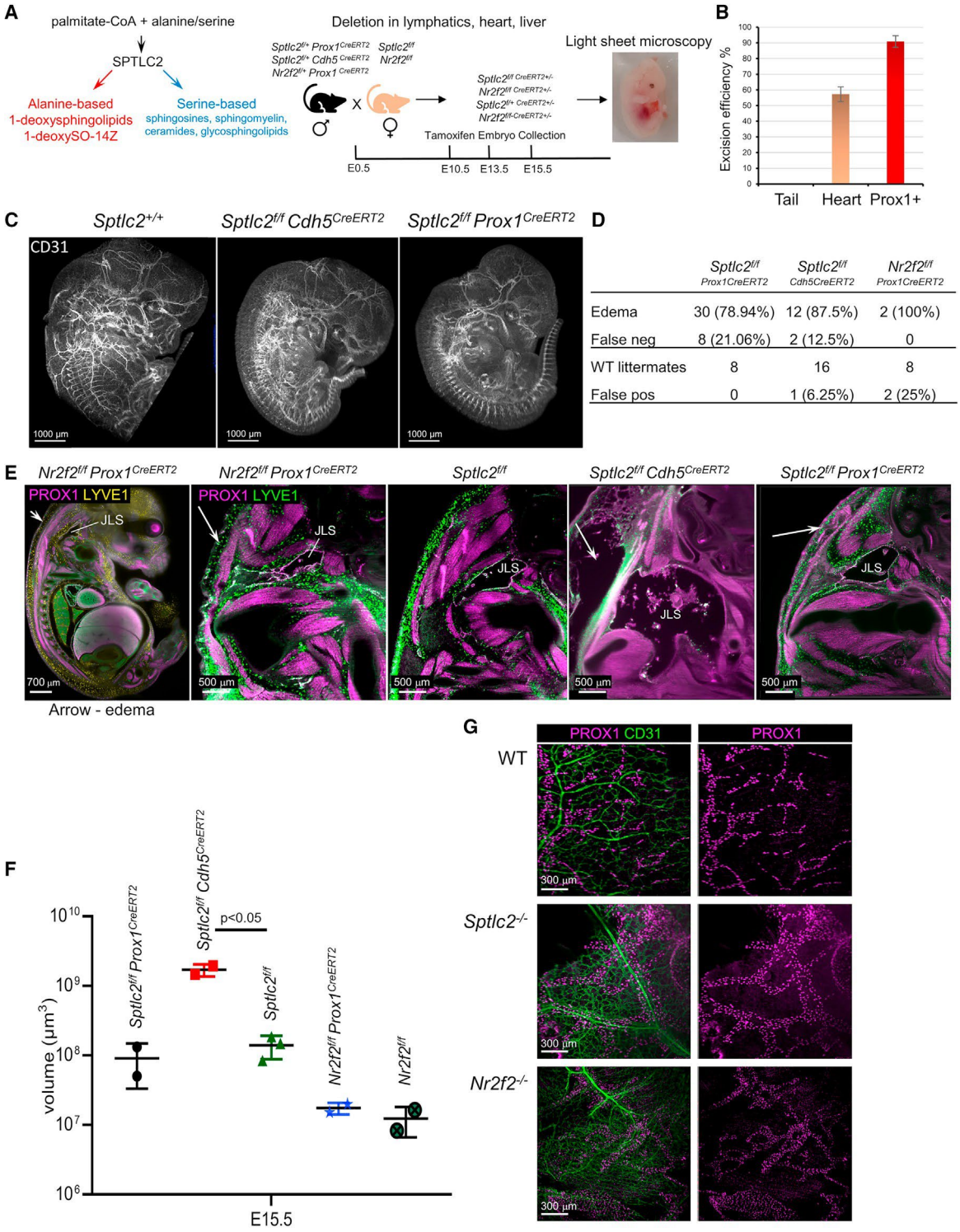

Figure 3. Phenotypes of *Sptlc2*$^{f/f}$ *Prox1*$^{Cre\text{-}ERT2/+}$ and *Sptlc2*$^{f/f}$ *Cdh5*$^{Cre\text{-}ERT2/+}$ embryos correlate to those of *Nr2f2* deficient animals

(A) Genetic manipulation of *Sptlc2*.

(B) Deletion efficiency of *Sptlc2*$^{f/f}$ in *Prox1*$^{Cre\text{-}ERT2/+}$ mice by genomic qPCR. Error bars are standard deviation.

(C) Surface rendering of blood vessels in E13.5 embryos.

(D) Summary of edema phenotype in *Sptlc2*$^{-/-}$ embryos.

(E) Edema in Nr2f2$^{-/-}$ and *Sptlc2*$^{-/-}$ embryos by light-sheet microscopy. Ortho slices (5 mm) of representative embryos (right panels).

(F) Comparison of JLS volume across the strains used in (E). Error bars are standard deviation.

(G) Blood vessel branching and dilated dermal lymphatics in Nr2f2$^{-/-}$ and *Sptlc2*$^{-/-}$ E15.5 embryos.

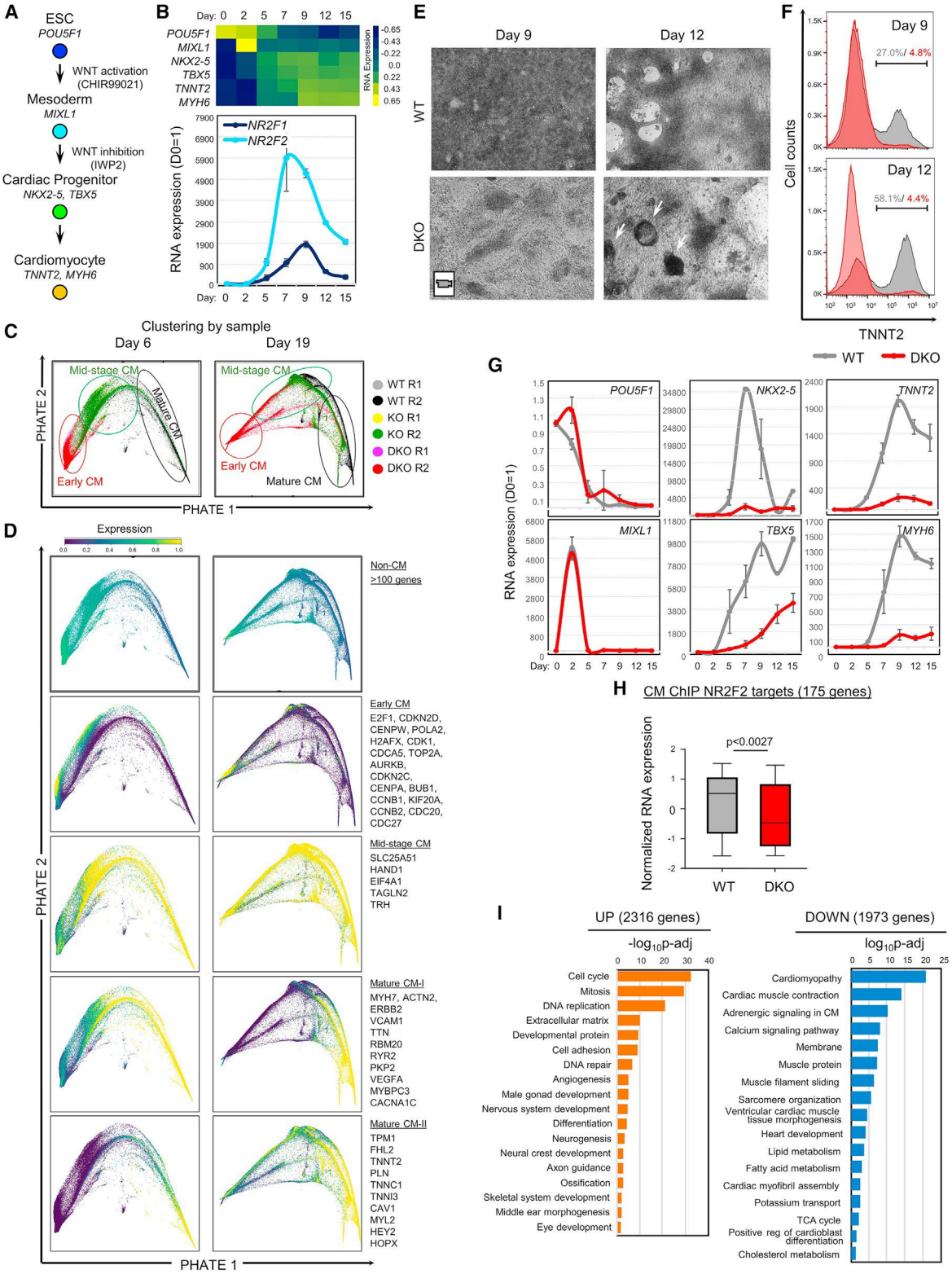

Figure 4. Simultaneous deletion of *NR2F1* and *NR2F2* negatively impacts cardiomyocyte differentiation

(A) CM differentiation protocol.

(B) Expression of *NR2F1* and *NR2F2* and key differentiation markers during CM differentiation. Error bars are standard error.

(C) Combined scRNA-seq data of CMs derived from WT, KO, and DKO hESCs.

(legend continued on next page)

et al., 2007, 2010). Edema was consistently observed in *Sptlc2*$^{f/f}$ *Prox1*$^{Cre\text{-}ERT2}$ (penetrance of 0.78), *Sptlc2*$^{f/f}$ *Cdh5*$^{Cre\text{-}ERT2}$ (penetrance 0.87), and *Nr2f2*$^{f/f}$ *Prox1*$^{Cre\text{-}ERT2}$ (penetrance 1) embryos at E15.5 (Figures 3D and S3A). Edema was visible by light-sheet microscopy (Figure 3E). We did not observe blood-filled lymphatics, even in the *Nr2f2* conditional knockout model.

Next, we investigated the development of the jugular lymphatic sac (JLS). Formation of the JLS begins around E10 when progenitors of lymphatic endothelial cells (LECs) emerge from the primitive iliac and cardinal veins (Srinivasan et al., 2007). The JLS morphology of *Sptlc2*$^{f/f}$ *Prox1*$^{Cre\text{-}ERT2}$ mice at E15.5 was relatively normal (Figure 3E) and similar to that reported for Nr2f2$^{-/-}$ *Prox1*^{CreERT2} mice (Srinivasan et al., 2007; Srinivasan and Oliver, 2011). In contrast, the *Sptlc2* and *Nr2f2* knockout phenotype was more severe in the *Cdh5*$^{Cre\text{-}ERT2}$ model, most likely due to the deletion of *Sptlc2* in all endothelial cells (Wang et al., 2010). Indeed, the JLS of the E13.5 *Sptlc2*$^{f/f}$ *Cdh5*$^{Cre\text{-}ERT2}$ embryos were more disorganized and volumetrically larger (Figures 3E and 3F) when compared with those from the *Prox1*^{CreERT2} models and controls (Figure 3F). No E15.5 *Nr2f2*$^{f/f}$ *Cdh5*$^{Cre\text{-}ERT2}$ embryos were obtained, suggesting embryonic lethality at an earlier stage. Furthermore, the dermal lymphatic networks of E15.5 embryos were altered (Figure 3G). In the WT embryos, the larger blood vessels branched to form a regular network of smaller vessels, while lymphatic vessels were narrow and well formed. In *Nr2f2*- and *Sptlc2*-deficient an- imals, the larger blood vessels branched less and instead formed a mesh-like capillary structure with bloated lymphatic vessels (Figure 3G), which is reminiscent of the *Nr2f2*$^{-/-}$ phenotype (Lin et al., 2010). These results suggest a correlation between the cardiac, vascular, and lymphatic endothelial phenotypes of *Sptlc2* and *Nr2f2* deficient embryos.

To test whether 1-deoxysphingosines could rescue the *Sptlc2*$^{-/-}$ phenotypes in mouse LECs, we used 4-hydroxy- tamoxifen (4OH-TMX) to delete floxed *Nr2f2*$^{f/f}$ *Prox1*^{CreERT2} or *Sptlc2*$^{f/f}$ *Prox1*^{CreERT2} alleles in primary cultures of mouse LECs (Figure S3B). The medium was supplemented with D-erythroSO to provide a precursor for the synthesis of canonical sphingolipids. We compared untreated cells with cells treated with 4OH-TMX combined with either a vehicle or 1-deoxySO-14Z. In the absence of 1-deoxySO-14Z, LECs in both *Nr2f2* and *Sptlc2* deleted cultures died between 24 and 48 h following 4OH-TMX administration. Addition of 1-deoxySO-14Z restored the number of viable cells in *Sptlc2*-deleted cultures, but not in *Nr2f2*-deleted cultures (Figure S3C). Within the 24-h interval after the 4OH-TMX administration, the presence of 1-deoxySO-14Z, but not the vehicle, partially restored PROX1 levels in LECs (Fig- ures S3D and S3E). Likely due to the short experimental time window, no effects were observed on other lymphatic endothe- lial markers, such as LYVE1 and NR2F2. Similarly, 1-deoxySO- 14Z partially rescued cardiac development in E10.5 embryo cultures of *Sptlc2*$^{f/f}$ *Cdh5*^{CreERT2} mice (Figures S3F and S3G).

Taken together, these results suggest that 1-deoxysphingosine could partially rescue the *Sptlc2*$^{-/-}$ phenotype in mouse LECs and embryonic hearts.

Sphingolipid biosynthesis modulates NR2F1/2-regulated transcription in human ESC-derived cardiomyocytes

To understand the link between sphingolipid biosynthesis and NR2F1/2-regulated transcription, we used cardiomyocytes differentiated from human embryonic stem cell (hESC) (CM). *NR2F2* plays a key role in CM maturation (Churko et al., 2018). During CM differentiation, *NR2F2* transcription was induced immediately after mesoderm specification concomitantly with the induction of cardiac progenitor factors *NKX2-5* and *TBX5* (Figures 4A and 4B). *NR2F1* was also induced with similar kinetics (Figure 4B) and was suggested to partially compensate for the loss of *NR2F2* during CM differentiation (Schwach et al., 2017). Since NR2F1 and NR2F2 share a common ligand, we used CRISPR-Cas9 gene editing to generate single NR2F2 knockout (KO) and NR2F1/2 double knockouts (DKO) hESCs (Figures S4A–S4C) to study the interplay between ligand biosynthesis and NR2F1/2-mediated transcription.

We characterized CM differentiation induced by modulation of the Wnt/b-catenin pathway (Lian et al., 2013) in WT, KO, and DKO cells. The cellular composition of CM cultures was analyzed by single-cell RNA sequencing (scRNA-seq) at early (day 6) and late (day 19) stages of CM maturation. Cell populations, where identified using the PHATE single-cell analysis pipeline (Moon et al., 2019) and segregated according to genotype (Figure 4C). DKO cells contributed little to clusters in the KO group and negligibly to clusters in the WT group. Likewise, the KO cells had limited contribution to clusters of WT or DKO samples (Figures S4D and S4E). We then compared the CM maturation states in the three cultures using previously defined CM cluster classification methods (Churko et al., 2018). At day 6, WT cultures contained cells of both intermediate and mature differentiation stages. In contrast, KO cultures contained cells of intermediate stages and DKO cultures predominantly contained cells of early proliferative stages with small numbers of mature-, mid-stage cells, and non-cardiac lineages (Figures 4C, 4D, S4D, and S4E). Mature CM cells were present in all cultures at day 19, albeit in reduced amounts in DKO cultures (Figure 4C).

The scRNA-seq data were validated by morphological examination of WT and DKO cultures. WT cultures consisted of dense sheets of cells with typical CM morphology and exhibited robust ''beating'' by day 9. DKO cultures were less dense, with few small ''beating'' clusters emerging by day 12 (Figure 4E; Videos S1, S2, S3, and S4). Cytometry profiling of the cultures showed a reduction in TNNT2^{+} CMs in DKO cultures (Figure 4F). qRT-PCR analyses of the stage-specific differentiation markers revealed that while both WT and DKO cells efficiently downregulated the pluripotency marker *POU5F1* and induced the mesodermal

(D) Distribution of mature-, mid-, and early-stage CM and non-CM populations in cells derived from WT, KO, and DKO hESCs.
(E) Morphology of CM cultures (days 9 and 12). Arrows: ''beating'' cell clusters in DKO cells.
(F) TNNT2 expression in CMs derived from WT and DKO hESCs.
(G) Expression of CM markers in WT and DKO cells defined by qPCR. Error bars are standard error.
(H) Expression of NR2F2 targets in WT and DKO CMs. Error bars are standard deviation. p-Value was determined using a two tailed Student's t test.
(I) GO analyses of genes up/downregulated in DKO cells (day 6).

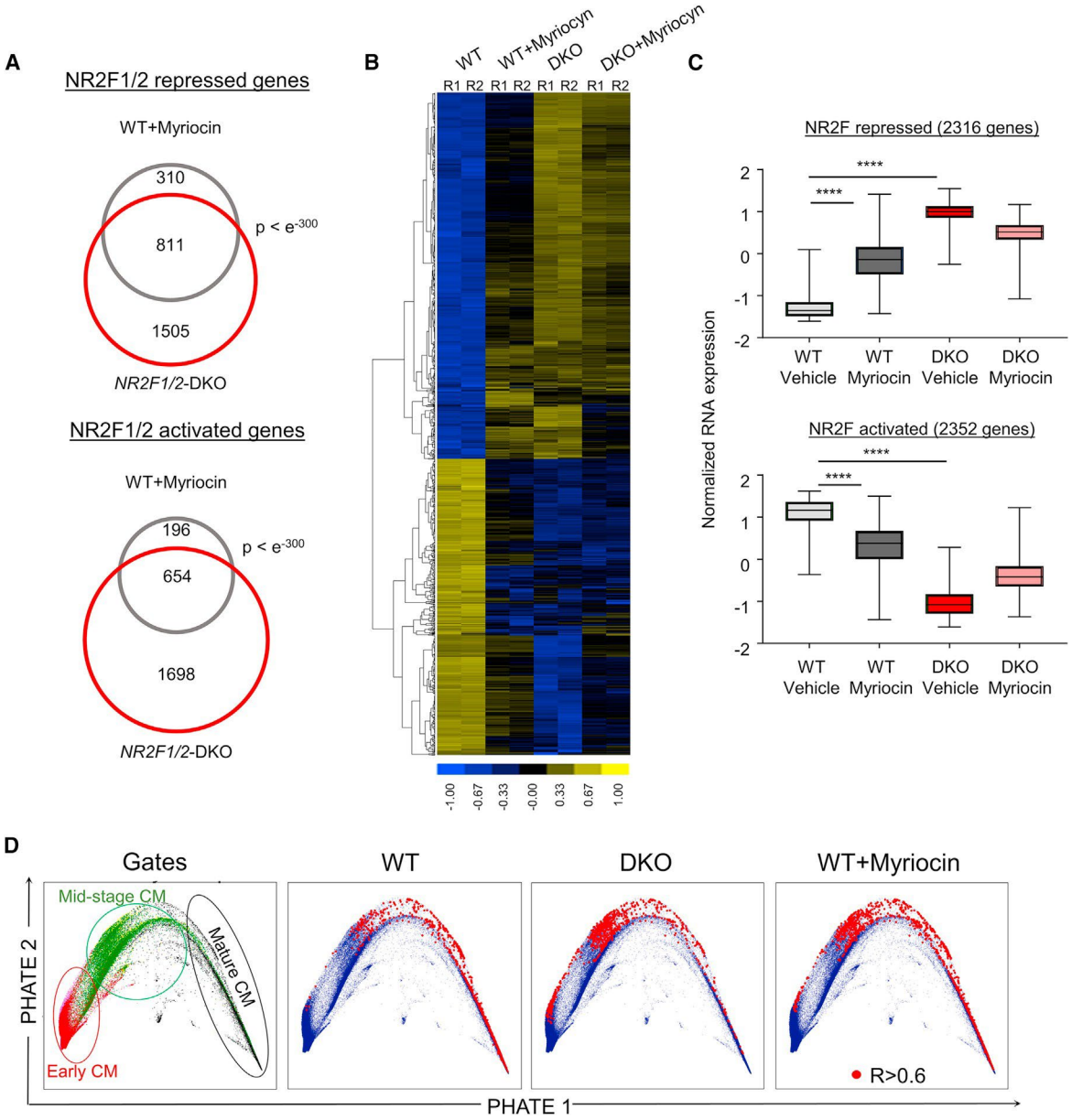

Figure 5. Sphingolipid biosynthesis modulates NR2F1/2-regulated gene network in hESC-derived cardiomyocytes

(A) Myriocin modulates NR2F1/2-dependent gene expression in day 6 CMs. p-Values were calculated using the hypergeometric distribution.

(B) Heatmap data from (A).

(C) Expression profiles of genes modulated by NR2F1/2 in day 6 CMs. Boxes denote second and third distribution quartiles, whiskers show the first and the fourth quartiles, the median is marked by horizontal line. p-values are from the Student's t test.****p values < 0.0001.

(D) Projection of bulk RNA-seq data from day 6 myriocin-treated cultures onto PHATE embedding. Red = cells with R > 0.6 correlation with corresponding bulk RNA-seq transcriptome.

marker *MIXL1*, cardiac progenitor specification and maturation was significantly delayed in DKO cultures (Figure 4G). Furthermore, a set of 175 curated NR2F2 ChIP targets (Churko et al., 2018) were significantly downregulated in DKO cells in comparison with WT cells (Figure 4H). Gene ontology (GO) analyses revealed that *NR2F1/2* deletion impacted CM specification program and cellular metabolism (Figure 4I). Day 6 DKO CM cultures exhibited deregulated expression of genes involved in sterol, fatty acid, glycerolipid, phospholipid, and sphingolipid metabolism (Figures 4I, S4F, and S4G). Inspection of day 12 *NR2F2*-KO cells by transmission electron microscopy revealed increased size and numbers of white lipid droplets as well as autophagosomes and lysosomes filled with membranous debris (Figure S4H). Taken together, our findings show that NR2F1/2 modulate CM differentiation and cellular lipid metabolism.

To test the link between sphingolipid biosynthesis and NR2F1/2-regulated transcription, we treated WT CM cultures with myriocin, a specific inhibitor of canonical and non-canonical

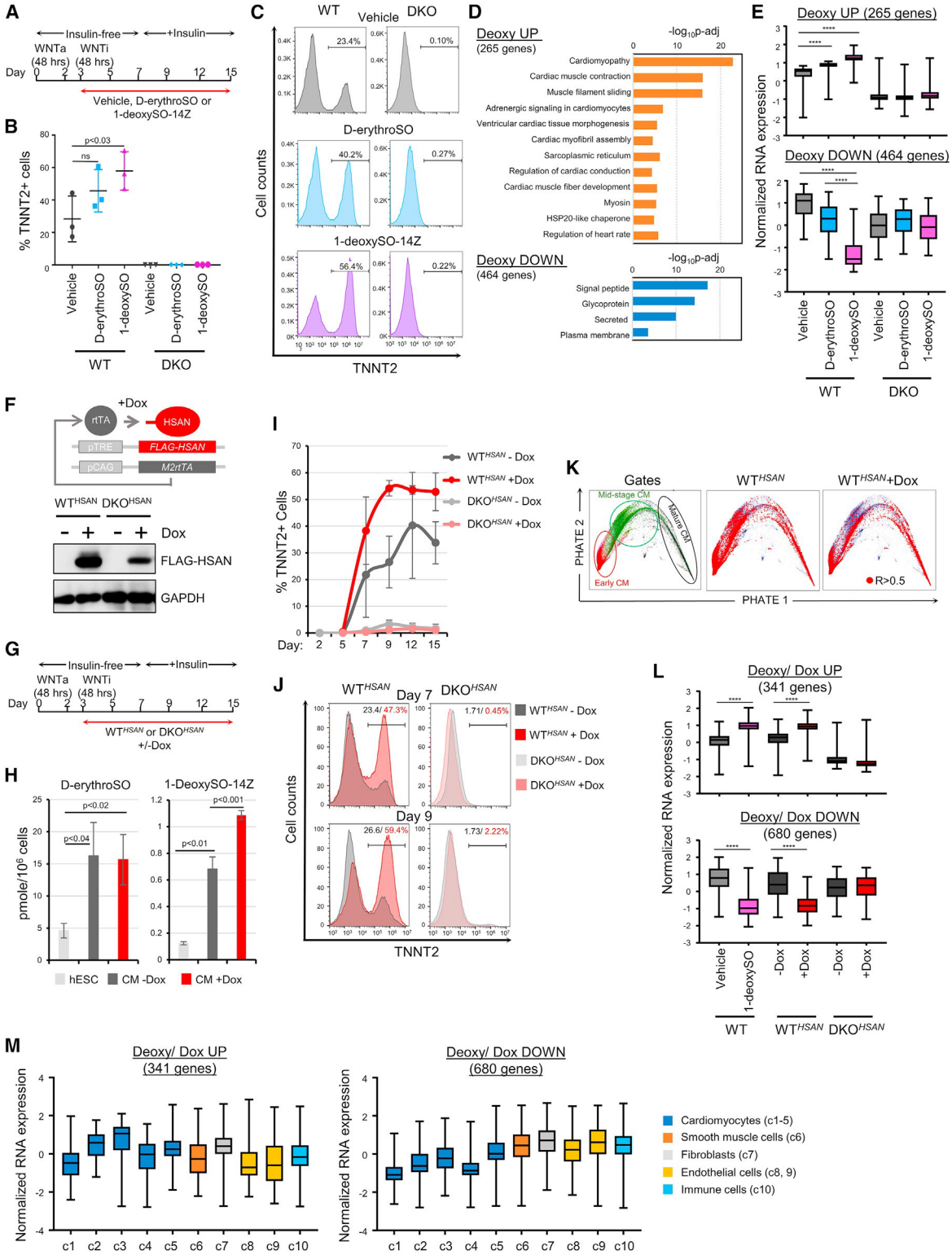

Figure 6. Exogenous and endogenous 1-deoxysphingosines modulate NR2F1/2-regulated transcription in human ESC-derived cardiomyocytes

(A) Schedule of ligand supplementation during CM differentiation.

(B) 1-deoxysphingosine supplementation increases the fraction of TNNT2+ cells. Error bars are standard deviation. p-Values were calculated using two tailed Student's t test.

(C) Representative FACS profiles of TNNT2 expression in WT and DKO CMs treated with vehicle, D-erythroSO and 1-deoxySO-14Z.

(legend continued on next page)

sphingolipid biosynthesis (Miyake et al., 1995). Myriocin was administered from day 1 at 1 mM concentration, an amount sufficient to partially suppress NR2F2 reporter activity in HEK-293FT cells without loss of cell viability (Figures S5A and S5B). Bulk RNA-seq analysis of myriocin-and vehicle-treated cultures at day 6 of differentiation identified 1,121 upregulated and 850 downregulated genes. A large fraction of genes up or downregulated by myriocin in WT cells were similarly affected in DKO cells. Importantly, these co-regulated genes were not similarly affected in myriocin-treated DKO cells, suggesting that inhibition of sphingolipid biosynthesis in WT cells phenocopies *NR2F2* deletion at the molecular level (Figures 5A and 5B). Notably, out of 175 previously identified direct targets of NR2F2 (Wu et al., 2013), 69 were upregulated and 15 downregulated in day 6 WT cultures when compared with DKO cultures, suggest- ing that NR2F1/2 is an activator during early CM specification (Figure S5C). Key transcriptional regulators of CM lineage specification (GATA4 and NKX2-5), as well as structural proteins of mature CMs (MYH6, MYBPC3, TNNT2, and MYBPC3) were among the upregulated NR2F1/2 targets (Figure S5D). The median expression of activated NR2F2 genes was significantly downregulated in myriocin-treated WT cultures but not in myriocin-treated DKO cultures (Figures 5C, S5C, and S5D). We correlated bulk RNA-seq data from WT, DKO, and myriocin-treated cultures with day 6 scRNA-seq data and found that the bulk transcriptome of myriocin-treated cultures exhibited the highest correlation with clusters of immature cells normally found in KO and DKO cultures (Figure 5D). This suggests that inhibition of sphingolipid biosynthesis mimics CM maturation defects arising from genetic deletion of *NR2F1/2*.

Exogenous or endogenous 1-deoxysphingosine supplementation activates NR2F1/2-regulated transcription in hESC-derived cardiomyocytes

Next, we tested the effect of sphingosines on CM differentiation by adding vehicle, D-erythroSO, or 1-deoxySO-14Z to WT or DKO cultures after the completion of mesoderm induction but before the emergence of NKX2-5$^+$ cardiac progenitors (Figure 6A). FACS analyses were performed at day 9, when NR2F1/2 expression peaked. Addition of 1-deoxysphingosine increased the fraction of TNNT2+ cells in WT cultures (Figures 6B and 6C) and modulated the expression of 265/464 genes by >2-fold (increases/decreases) when compared with vehicle-treated cultures (Figures 6D and 6E). Upregulated gene list was enriched for gene ontologies associated with CM matura- tion, while downregulated genes were enriched for secreted and membrane-bound proteins (Figure 6D). Notably, 160 out of 265 genes (~60%) upregulated in 1-deoxysphingosine-treated WT cultures were also NR2F1/2-activated genes. Among the genes upregulated by 1-deoxysphingosine were 33 NR2F2 ChIP targets including the key CM-specific targets *NKX2-5*, *MYBPC3*, *TNNT2*, and *MYH6* (Figures S6A and S6B). In contrast, genes downregulated in 1-deoxysphingosine-treated WT cul- tures overlapped poorly with NR2F1/2-repressed genes. Only 20 out of 464 downregulated genes (~4%) were NR2F1/2-repressed genes. These numbers suggest that 1-deoxysphingosine activated CM differentiation and maturation programs by modulating NR2F1/2 activity but inhibited expression of secretory genes independently of NR2F1/2 (Figure S6A).

The canonical sphingosine, D-erythroSO, also influenced CM differentiation and maturation, but gene expression changes in WT cultures treated with this sphingosine were smaller in magnitude than those induced by 1-deoxysphingosine (Figures 6B, 6C, 6E, S6A, and S6B). This finding agrees with our binding and activity data, which showed that D-erythroSO bound to NR2F2 at nanomolar concentrations but was a less efficient agonist when compared with 1-deoxySO-14Z (Figure 2). Impor- tantly, treatment of DKO cultures with either 1-deoxySO-14Z or D-erythroSO did not increase the fraction of TNNT2+ cells and minimally affected gene expression (Figures 6B, 6C, 6E, S6A, and S6B). Thus, our data indicate that the uptake of exogenous 1-deoxysphingosine by differentiating CMs increased the numbers of mature CMs in culture at least in part by modulating NR2F1/2-dependent transcriptional networks.

Next, we investigated whether autocrine production of 1-deoxysphingosines could modulate NR2F1/2-dependent transcription during CM differentiation. Levels of 1-deoxysphingosines and D-erythro-sphingosine were regulated during differentiation (Figure 6H). In day 7 CM cultures, levels of 1-deoxysphingosines reached 0.68 pmol/10^6 cells, which corresponds to 680 nM concentration, above the Kd measured by *in vitro* binding assays. To further increase the levels of 1-deoxysphingosines in differentiating CMs, we took advantage of the mutant version of the SPTLC1 enzyme (SPTLC1^{C133W}), which is associated with hereditary sensory and autonomic neuropathy type 1 (HSAN1) and increases production of 1-deoxysphingosines (Garofalo et al., 2011). We used TALEN-mediated gene targeting to integrate Doxycycline (Dox)-inducible *FLAG-SPTLC1^{C133W}* (hereafter *HSAN*) and rtTA transgenes into a constitutively active *AAVS1* locus of WT and DKO hESCs (Figures 6F and S6C). Transgene expression was induced by adding Dox to cultures at day 3, thus allowing a direct comparison of the same cell clone with or without induction of HSAN expression (Figure 6G).

The induction of *HSAN* by Dox increased 1-deoxysphingosine concentration in differentiating CM cultures by nearly 2-fold but minimally affected the metabolism of canonical sphingosines,

(D) Summary of GO analysis of genes up/downregulated by 1-deoxysphingosine in day 9 WT CM cultures.
(E) Expression profiles of up/downregulated genes in day 9 CMs after treatment with vehicle, D-erythroSO or 1-deoxysphingosine.
(F) The reverse tetracycline-controlled transactivator (rtTA) and *SPTLC1^{C133W}* (*HSAN1*) transgenes were integrated into the AAVS1 locus, protein expression induced by Dox analyzed by WB.
(G) Schedule of Dox supplementation during CM differentiation.
(H) Quantitation of canonical and non-canonical sphingosines in hESCs and day 7 CMs.
(I) Effect of *HSAN* expression on % of TNNT2+ cells in WT^{HSAN} and DKO^{HSAN} CMs during the 15-day differentiation time-course.
(J) Representative FACS profiles of TNNT2 expression in WT^{HSAN} and DKO^{HSAN} CM cultures.
(K) Projection of bulk RNA-seq data from day 7 WT^{HSAN} cultures onto the day 6 PHATE embedding.
(L) Genes up/downregulated after addition of 1-deoxysphingosine or Dox. ****p values < 0.0001.
(M) Genes up/downregulated after addition of 1-deoxysphingosine or Dox in different cell types of the human heart.

amino acids, fatty acids, ceramides, and sphingosine-1-phosphate (Figures 6H, S6D, and S6E). Induction of *HSAN* did decrease the levels of palmitic acid, a precursor of 1-deoxysphingosine, and other palmitic acid derivatives, such as palmitoyl-carnitine (Figure S6E). Thus, the introduction of the *HSAN* mutant specifically targeted 1-deoxysphingosine production and did not affect the general metabolism of cells.

Expression of *HSAN* increased the fraction of TNNT2+ cells in WT^{HSAN} cultures, similar to what was observed with 1-deoxysphingosine supplemented medium (Figures 6I and 6J). The bulk transcriptome of untreated day 7 WT^{HSAN} cultures correlated with early immature and mature CM clusters in single-cell PHATE embedding. In contrast, Dox-treated WT^{HSAN} cultures were depleted of immature CMs, suggesting that elevated 1-deoxysphingosine levels accelerate CM maturation (Figure 6K). Transcriptome analyses of DOX-treated cultures at day 7 and 9 identified 301/392 genes with more than 2-fold increases/decreases in expression levels. Dox-treated WT^{HSAN} cultures and WT cultures supplemented with 1-deoxysphingosine exhibited similar profiles of up- and downregulated genes, including those of CM-specific NR2F2 targets (Figures 6L, S6B, and S6F). Reflective of these similarities, the enriched gene ontologies of Dox-treated WT^{HSAN} cultures mirrored those of 1-deoxysphingosine treated WT samples. Specifically, genes associated with CM differentiation or maturation were overrepresented in the upregulated gene list, whereas secreted and membrane proteins were overrepresented in the downregulated gene list (Figure S6G). Importantly, *HSAN* expression in differentiating DKO CMs failed to increase the fraction of TNNT2+ cells and had a minimal effect on overall gene expression (Figures 6I, 6J, 6L, and S6F).

The negligible overlap of genes downregulated by *HSAN*/1-deoxysphingosine and NR2F1/2-repression suggests that 1-deoxysphingosine could have both NR2F1/2 dependent and independent effects on CM differentiation (Figure S6A). Genes downregulated by HSAN/1-deoxysphingosine were enriched in secreted proteins not typically expressed by CMs (Fig- ure S6G). Thus, 1-deoxysphingosines could be suppressing differentiation of mesoderm-derived non-CM cells. To test this hypothesis, we calculated median expression levels of genes up- or downregulated by *HSAN* and/or 1-deoxysphingo- sines in different cell types of the human heart using single-cell data from the Human Protein Atlas Project (Uhle´ n et al., 2015). Indeed, expression of upregulated genes was higher in CM clusters, whereas downregulated genes were associated with fibroblasts, endothelial, smooth muscle, and immune cells (Figure 6M).

Our data collectively support the conclusion that 1-deoxysphingosines are developmentally regulated metabolites that activate NR2F1/2-dependent CM differentiation and maturation programs and inhibit differentiation of non-CM lineages independently of NR2F1/2.

DISCUSSION

We identified 1-deoxysphingolipids as modulators of NR2F1/2 using an approach consisting of two sequential screens. In the first screen, a comprehensive library of metabolic enzymes was overexpressed to identify metabolic pathways that modulate NR2F1/2 reporter activity in mammalian cells. For the second filter, substrates and products of these pathways were evaluated for their ability to activate NR2F1/2-dependent transcription in *D. melanogaster* cells, resulting in the identification of 1-deoxysphingolipids as NR2F1/2 modulators. Our approach is unbiased and makes no assumption of ligand structure and could be adapted to identify ligands of other orphan NHRs.

Data from the overexpression screen suggest that in addition to sphingolipid biosynthesis, which directly controls ligand production, three additional metabolic pathways, including amino acid, fatty acid, and iron-sulfur cluster metabolism, may indirectly regulate ligand synthesis. Indeed, iron depletion affects sphingolipid biosynthesis in yeast (Lee et al., 2012b; Sha- koury-Elizeh et al., 2010), and fatty acid metabolism provides precursors for sphingolipid biosynthesis (Merrill et al., 1988). Amino acid metabolism controls the availability of serine, alanine, and glycine for sphingolipid biosynthesis (Esaki et al., 2015). Furthermore, the overexpression screen suggests that the components of the SPTLC complex play different roles in ligand synthesis. The SPTLC complex has three enzymatic subunits: SPTLC1, SPTLC2, or SPTLC3. SPTLC1 is the common component of the complex, while SPTLC2 and SPTLC3 modulate its specificity for fatty acids (Lone et al., 2020; Russo et al., 2013). Complexes with SPTLC1-SPTLC2 subunits generate sphingolipids with 18, 19, and 20 carbon bases (Lone et al., 2020), which agrees with our finding that SPTLC2 is the only component of sphingolipid biosynthesis that increased NR2F1/2 transcriptional activity.

The Kd range of 10–100 nM for *in vitro* binding and cell- based assays fits with the concentration ranges of 1-deoxysphingosines found in lymphatic endothelial cell lines and CM cultures and suggests that these ligands could be physiological. In contrast, canonical sphingolipids such as D-erythroSO bind to NR2F1/2-LBD with an affinity slightly lower than that of 1-deoxysphingosines but are either weak agonists of NR2F1/2 or inactive. Such a discrepancy between binding and activity could be due to the low availability of free canonical sphingosines, which are precursors for all other cellular sphingolipids (Merrill, 2011).

Unexpectedly, while mammalian cells exhibit NR2F1/2 transcriptional activity in the absence of added ligand, no basal Svp or NR2F1/2 transcriptional activity was observed in *D. melanogaster* S2 cells. This finding is surprising as mammalian and fly NR2F1/2 homologs share 92% identity (Tsai and Tsai, 1997), and most amino acid residues facing the ligand-binding pocket are conserved, suggesting that COUP-TFs of vertebrates and insects are under strong evolutionary pressure to bind the same ligand. Based on the lack of activity in fly tissues and cell lines, previous studies proposed that Svp is a repressor (Palanker et al., 2006). Our findings, however, suggest that Svp is transcriptionally active in fly cells in the presence of 1-deoxysphingosines. The most plausible explanation for this discrepancy is that the ligand is not produced by the insect cell line utilized in our study but is generated by the few Svp-expressing cells *in vivo*. Most mammalian sphingolipids, including the NR2F1/2 ligands identified here, have sphingoid bases with 18 to 20 carbons, while flies preferentially make C14 and C16 sphingolipids (Fyrst et al., 2004, 2008). Despite this preference, small amounts of

mammalian-like C18 and C20 sphingolipids are made in a tissue-specific manner in *D. melanogaster* (Fyrst et al., 2004) and C18 sphingolipids with 0, 1, or 2 double bonds are enriched in *Sply* mutant flies, which are deficient in sphingolipid catabolism (Narayanaswamy et al., 2014). The identification of conditions for tissue-specific production of C18 and C20 deoxysphingosines in flies could shed light on the role of Svp in the development of *D. melanogaster*.

Our data support the conclusion that 1-deoxysphingolipids are activators of NR2F1/2-mediated transcription. However, others suggested that NR2F1/2 may also function as transcrip- tional repressors (Churko et al., 2018; Wu et al., 2013). Given that 1-deoxysphingosines can be further modified by CYP450 enzymes to generate new metabolites (Alecu et al., 2017), it would be important to test whether these derivatives could func- tion as NR2F1/2 agonists or antagonists. Indeed, in the case of FXR, a receptor for bile acids, natural agonists (Makishima et al., 1999; Parks et al., 1999) and antagonists (Sayin et al., 2013) have been found. These show a range of biological activ- ities from the regulation of intestinal stem cells to facilitating tu- mor development (Fu et al., 2019).

The modulation of CM differentiation and maturation by 1-deoxysphingosines is largely NR2F1/2 dependent, but the inhibition of non-CM differentiation programs appears to engage mechanisms that are independent of NR2F1/2. Indeed, similar effects have been reported for other NHR ligands. For example, estrogen, a ligand for ERa and ERb, also activates the G-protein-coupled receptor (GPCR) GPER (Revankar et al., 2005). Similarly, bile acids bind to both FXR (Makishima et al., 1999; Parks et al., 1999) and the GPCR TGR5 (Kawamata et al., 2003). The mechanism behind NR2F1/2-independent functions of 1-deoxysphingosines remains to be elucidated.

Previous studies documented the cytotoxic nature of 1-deoxysphingosines accumulating in tissues and causing HSAN1 and macular degeneration (Eichler et al., 2009; Gantner et al., 2019; Penno et al., 2010; Rotthier et al., 2010). Our findings, however, suggest an alternative model where overproduction of 1-deoxysphingosines in disease engages normal gene regulatory networks induced by the autocrine or hormone-like function of 1-deoxysphingosine. An analogous situation is observed in autosomal aldosteronism, a disease that is characterized by hypertension and caused by mutations that induce the ectopic expression of aldosterone synthase, leading to increased levels of mineralocorticoids and chronic stimulation of the mineralocorticoid receptor (Lifton et al., 1992). So far, the link between the pathology induced by 1-deoxysphingosines and NR2F1/2 transcriptional activity has not been established. Our findings highlight the importance of identifying the natural ligands of NHRs to enhance our understanding of human physiology.

Limitations of the study

Sphingolipids elicit concentration dependent effects in aqueous solutions (Sasaki et al., 2009). This limits the bioavailability and working concentrations of these lipids in cell-based assays and *in vitro* binding assays. Furthermore, ligand-receptor studies *in vivo* were limited by time constrains as primary LECs, and embryos *ex vivo* only survive for short periods after deletion of *Sptlc2*. The small amounts of tissues and cells in embryos limited our ability to measure the concentrations of 1-deoxysphingosines in embryonic tissues that express NR2F1/2. Thus, embryo phenotypes are mostly correlative. While the use of *in vitro* CM differentiation model provided a solution for some of these limitations, methods to study the receptor- ligand relationship *in vivo* should provide further support for our findings.

STAR+METHODS

Detailed methods are provided in the online version of this paper and include the following:

- KEY RESOURCES TABLE
- RESOURCE AVAILABILITY
  - Lead contact
  - Material availability
  - Data and code availability
- EXPERIMENTAL MODEL AND SUBJECT DETAILS
- METHOD DETAILS
  - Insect and mammalian reporter systems
  - Enzyme overexpression screening
  - Metabolite screening
  - Preparation of sphingolipid–BSA complexes
  - Reporter assays in mammalian cells
  - Reporter assays in insect cells
  - Cell-based reporter assays for sphingolipids in mammalian cells
  - Immunoprecipitation and lipidomics
  - Sphingolipidome of TIME cells
  - Targeted metabolomics
  - Amino acids
  - Sphingolipids
  - Fatty acids
  - Purification of bacterial NR2F1 and NR2F2 LBDs
  - Purification of mammalian NR2F2 LBDs
  - Fluorescence polarization assay (FPA)
  - Thermal shift assays using recombinant NR2F2-LBD
  - Surface plasmon resonance (SPR)
  - Conditional deletion of *Sptlc2* and *Nr2f2* in mice
  - Deletion efficiency after tamoxifen injection
  - Embryo processing, staining, and imaging
  - Rescue experiments using mouse lymphatic endothelium
  - Rescue experiments using ex-vivo embryo culture
  - Generation of *NR2F2*-KO and *NR2F1/2*-dKO hESC lines
  - Generation of Dox-inducible *SPTLC1*^{C133W} (*HSAN*) hESC lines
  - Cardiomyocyte differentiation of hESCs
  - TNNT2 staining of cardiomyocytes
  - Electron microscopy of hESC-derived cardiomyocytes
  - RNA isolation
  - Reverse Transcription and quantitative PCR (RT-qPCR)
  - Immunoblotting
  - Basic statistical analyses
  - Bulk RNA-seq analyses
  - Single-cell (sc)RNAseq of cardiomyocyte differentiation and data analyses

SUPPLEMENTAL INFORMATION

Supplemental information can be found online at https://doi.org/10.1016/j.devcel.2021.10.018.

ACKNOWLEDGMENTS

We thank Nancy Ruddle (Yale University), Benjamin S. Lowry, and Harrison B. Chong (University of Georgia) for critical reading of the manuscript, Vishwa Deep Dixit (Yale University) for Sptlc2 mice, Robert G. Kelly (IBDM, Marseille) for analysis of heart phenotype in Sptlc2 deficient animals, Christopher Castaldi and Guilin Wang (Yale Center for Genome Analysis) for RNA-seq and scRNA-seq, Bill Webb (the Scripps Center for Mass Spectrometry and Metabolomics) for LC-MS, Narinder Ghumman (University of Georgia) for bioinformatics, Timothy Nottoli (Yale University) for mouse rederivation, and Nikhil Joshi (Yale University) for help with mouse protocols. Mice were provided by MMRRC (*Nr2f2*$^{f/f}$) and Cancer Research UK (*Prox1-CreERT2* and *Cdh5-CreERT2*). The work was supported by NIH grants R21-AI131015 (F.R.S./S.M.K.), R01 GM107092 (N.B.I.), and R24GM137782 (P.A.), the Yale University institutional grant YD000234 (F.R.S.), CT RMRF grant 16-RMB-Yale-07 (S.K./N.B.I.), French National Research Agency grants ANR-16-ACHN-0011 and ANR-17-CE13-0029 (S.A.v.d.P.), FRM Amorcage de jeunes equipes AJE20150633331 (S.A.v.d.P.), the Swiss National Foundation grant project 31003A-179371 (T.H.), and the National Natural Science Foundation of China project 81600093 (T.W.).

AUTHOR CONTRIBUTIONS

Conceptualization, methodology, writing, review, and editing, F.R.S. and N.B.I. Supervision and project administration, F.R.S., N.B.I., and S.M.K. Investigation and validation, T.W., L.d.F., Z.W., J.T., B.R.R., B.J., T.Z., A.G., Zhirui Wang, P.A., S.X., M.P., D.E.S., T.H., C.A., E.M.S., I.A., S.A.v.d.P., N.B.I., and F.R.S. Resources, Zheng Wang, J.T., T.H., C.A., E.M.S., and I.A. Formal data analysis and curation, N.B.I., B.R.R., H.J.-L., D.B., and S.K.

DECLARATION OF INTERESTS

The authors declare no competing interests.

Received: August 2, 2020
Revised: August 30, 2021
Accepted: October 19, 2021
Published: November 10, 2021

REFERENCES

Al Turki, S., Manickaraj, A.K., Mercer, C.L., Gerety, S.S., Hitz, M.P., Lindsay, S., D'Alessandro, L.A., Swaminathan, G.J., Bentham, J., Arndt, A.K., et al. (2014). Rare variants in NR2F2 cause congenital heart defects in humans. Am. J. Hum. Genet. *94*, 574–585. https://doi.org/10.1016/j.ajhg.2014.03.007.

Alecu, I., Othman, A., Penno, A., Saied, E.M., Arenz, C., von Eckardstein, A., and Hornemann, T. (2017). Cytotoxic 1-deoxysphingolipids are metabolized by a cytochrome P450-dependent pathway. J. Lipid Res. *58*, 60–71. https://doi.org/10.1194/jlr.M072421.

Bazigou, E., Lyons, O.T., Smith, A., Venn, G.E., Cope, C., Brown, N.A., and Makinen, T. (2011). Genes regulating lymphangiogenesis control venous valve formation and maintenance in mice. J. Clin. Invest. *121*, 2984–2992. https://doi.org/10.1172/JCI58050.

Bosch, D.G., Boonstra, F.N., Gonzaga-Jauregui, C., Xu, M., de Ligt, J., Jhangiani, S., Wiszniewski, W., Muzny, D.M., Yntema, H.G., Pfundt, R., et al. (2014). NR2F1 mutations cause optic atrophy with intellectual disability. Am. J. Hum. Genet. *94*, 303–309. https://doi.org/10.1016/j.ajhg.2014.01.002.

Burkhardt, D.B., Stanley, J.S., Perdigoto, A.L., Gigante, S.A., Herold, K.C., Wolf, G., Giraldez, A.J., van Dijk, D., and Krishnaswamy, S. (2019). Quantifying the effect of experimental perturbations in single-cell RNA-sequencing data using graph signal processing. bioRxiv. https://doi.org/10.1101/532846.

Burridge, P.W., Matsa, E., Shukla, P., Lin, Z.C., Churko, J.M., Ebert, A.D., Lan, F., Diecke, S., Huber, B., Mordwinkin, N.M., et al. (2014). Chemically defined generation of human cardiomyocytes. Nat. Methods *11*, 855–860. https://doi.org/10.1038/nmeth.2999.

Churko, J.M., Garg, P., Treutlein, B., Venkatasubramanian, M., Wu, H., Lee, J., Wessells, Q.N., Chen, S.Y., Chen, W.Y., Chetal, K., et al. (2018). Defining human cardiac transcription factor hierarchies using integrated single-cell heterogeneity analysis. Nat. Commun. *9*, 4906. https://doi.org/10.1038/s41467-018-07333-4.

Eichler, F.S., Hornemann, T., McCampbell, A., Kuljis, D., Penno, A., Vardeh, D., Tamrazian, E., Garofalo, K., Lee, H.J., Kini, L., et al. (2009). Overexpression of the wild-type SPT1 subunit lowers desoxysphingolipid levels and rescues the phenotype of HSAN1. J. Neurosci. *29*, 14646–14651. https://doi.org/10.1523/JNEUROSCI.2536-09.2009.

Eppig, J.T. (2017). Mouse genome informatics (MGI) resource: genetic, genomic, and biological KnowledgeBase for the laboratory mouse. ILAR J *58*, 17–41. https://doi.org/10.1093/ilar/ilx013.

Esaki, K., Sayano, T., Sonoda, C., Akagi, T., Suzuki, T., Ogawa, T., Okamoto, M., Yoshikawa, T., Hirabayashi, Y., and Furuya, S. (2015). L-serine deficiency elicits intracellular accumulation of cytotoxic deoxysphingolipids and lipid body formation. J. Biol. Chem. *290*, 14595–14609. https://doi.org/10.1074/jbc.M114.603860.

Folch, J., Lees, M., and Sloane Stanley, G.H. (1957). A simple method for the isolation and purification of total lipides from animal tissues. J. Biol. Chem. *226*, 497–509.

Fu, T., Coulter, S., Yoshihara, E., Oh, T.G., Fang, S., Cayabyab, F., Zhu, Q., Zhang, T., Leblanc, M., Liu, S., et al. (2019). FXR regulates intestinal cancer stem cell proliferation. Cell *176*, 1098–1112.e18. https://doi.org/10.1016/j.cell.2019.01.036.

Fyrst, H., Herr, D.R., Harris, G.L., and Saba, J.D. (2004). Characterization of free endogenous C14 and C16 sphingoid bases from Drosophila melanogaster. J. Lipid Res. *45*, 54–62. https://doi.org/10.1194/jlr.M300005-JLR200.

Fyrst, H., Zhang, X., Herr, D.R., Byun, H.S., Bittman, R., Phan, V.H., Harris, G.L., and Saba, J.D. (2008). Identification and characterization by electrospray mass spectrometry of endogenous Drosophila sphingadienes. J. Lipid Res. *49*, 597–606. https://doi.org/10.1194/jlr.M700414-JLR200.

Gantner, M.L., Eade, K., Wallace, M., Handzlik, M.K., Fallon, R., Trombley, J., Bonelli, R., Giles, S., Harkins-Perry, S., Heeren, T.F.C., et al. (2019). Serine and lipid metabolism in macular disease and peripheral neuropathy. N. Engl. J. Med. *381*, 1422–1433. https://doi.org/10.1056/NEJMoa1815111.

Garofalo, K., Penno, A., Schmidt, B.P., Lee, H.J., Frosch, M.P., von Eckardstein, A., Brown, R.H., Hornemann, T., and Eichler, F.S. (2011). Oral L-serine supplementation reduces production of neurotoxic deoxysphingolipids in mice and humans with hereditary sensory autonomic neuropathy type 1. J. Clin. Invest. *121*, 4735–4745. https://doi.org/10.1172/JCI57549.

Gauchat, D., Escriva, H., Miljkovic-Licina, M., Chera, S., Langlois, M.C., Begue, A., Laudet, V., and Galliot, B. (2004). The orphan COUP-TF nuclear receptors are markers for neurogenesis from cnidarians to vertebrates. Dev. Biol. *275*, 104–123. https://doi.org/10.1016/j.ydbio.2004.07.037.

Giguere, V., Ong, E.S., Segui, P., and Evans, R.M. (1987). Identification of a receptor for the morphogen retinoic acid. Nature *330*, 624–629. https://doi.org/10.1038/330624a0.

Hanada, K., Nishijima, M., Kiso, M., Hasegawa, A., Fujita, S., Ogawa, T., and Akamatsu, Y. (1992). Sphingolipids are essential for the growth of Chinese hamster ovary cells. Restoration of the growth of a mutant defective in sphingoid base biosynthesis by exogenous sphingolipids. J. Biol. Chem. *267*, 23527–23533.

Hermann-Kleiter, N., Gruber, T., Lutz-Nicoladoni, C., Thuille, N., Fresser, F., Labi, V., Schiefermeier, N., Warnecke, M., Huber, L., Villunger, A., et al. (2008). The nuclear orphan receptor NR2F6 suppresses lymphocyte activation and T helper 17-dependent autoimmunity. Immunity *29*, 205–216. https://doi.org/10.1016/j.immuni.2008.06.008.

Hermann-Kleiter, N., Meisel, M., Fresser, F., Thuille, N., Mu€ller, M., Roth, L., Katopodis, A., and Baier, G. (2012). Nuclear orphan receptor NR2F6 directly

antagonizes NFAT and RORgt binding to the Il17a promoter. J. Autoimmun. *39*, 428–440. https://doi.org/10.1016/j.jaut.2012.07.007.

Heyman, R.A., Mangelsdorf, D.J., Dyck, J.A., Stein, R.B., Eichele, G., Evans, R.M., and Thaller, C. (1992). 9-cis retinoic acid is a high affinity ligand for the retinoid X receptor. Cell *68*, 397–406.

Hornemann, T., Penno, A., Ru€tti, M.F., Ernst, D., Kivrak-Pfiffner, F., Rohrer, L., and von Eckardstein, A. (2009). The SPTLC3 subunit of serine palmitoyltransferase generates short chain sphingoid bases. J. Biol. Chem. *284*, 26322–26330. https://doi.org/10.1074/jbc.M109.023192.

Huh, J.R., Leung, M.W., Huang, P., Ryan, D.A., Krout, M.R., Malapaka, R.R., Chow, J., Manel, N., Ciofani, M., Kim, S.V., et al. (2011). Digoxin and its derivatives suppress TH17 cell differentiation by antagonizing RORgt activity. Nature *472*, 486–490. https://doi.org/10.1038/nature09978.

Janowski, B.A., Willy, P.J., Devi, T.R., Falck, J.R., and Mangelsdorf, D.J. (1996). An oxysterol signalling pathway mediated by the nuclear receptor LXR alpha. Nature *383*, 728–731. https://doi.org/10.1038/383728a0.

Jonk, L.J., de Jonge, M.E., Pals, C.E., Wissink, S., Vervaart, J.M., Schoorlemmer, J., and Kruijer, W. (1994). Cloning and expression during development of three murine members of the COUP family of nuclear orphan receptors. Mech. Dev. *47*, 81–97.

Jordan-Williams, K.L., and Ruddell, A. (2014). Culturing purifies murine lymph node lymphatic endothelium. Lymphat. Res. Biol. *12*, 144–149. https://doi.org/10.1089/lrb.2013.0053.

Kanai, M.I., Okabe, M., and Hiromi, Y. (2005). Seven-up controls switching of transcription factors that specify temporal identities of Drosophila neuroblasts. Dev. Cell *8*, 203–213. https://doi.org/10.1016/j.devcel.2004.12.014.

Kanatani, S., Honda, T., Aramaki, M., Hayashi, K., Kubo, K., Ishida, M., Tanaka, D.H., Kawauchi, T., Sekine, K., Kusuzawa, S., et al. (2015). The COUP-TFII/Neuropilin-2 is a molecular switch steering diencephalon-derived GABAergic neurons in the developing mouse brain. Proc. Natl. Acad. Sci. USA *112*, E4985–E4994. https://doi.org/10.1073/pnas.1420701112.

Kanehisa, M., Furumichi, M., Tanabe, M., Sato, Y., and Morishima, K. (2017). KEGG: new perspectives on genomes, pathways, diseases and drugs. Nucleic Acids Res *45*, D353–D361. https://doi.org/10.1093/nar/gkw1092.

Kawamata, Y., Fujii, R., Hosoya, M., Harada, M., Yoshida, H., Miwa, M., Fukusumi, S., Habata, Y., Itoh, T., Shintani, Y., et al. (2003). A G protein-coupled receptor responsive to bile acids. J. Biol. Chem. *278*, 9435–9440. https://doi.org/10.1074/jbc.M209706200.

Kruse, S.W., Suino-Powell, K., Zhou, X.E., Kretschman, J.E., Reynolds, R., Vonrhein, C., Xu, Y., Wang, L., Tsai, S.Y., Tsai, M.J., and Xu, H.E. (2008). Identification of COUP-TFII orphan nuclear receptor as a retinoic acid-activated receptor. PLoS Biol *6*, e227. https://doi.org/10.1371/journal.pbio.0060227.

Le Gue´ vel, R., Oger, F., Martinez-Jimenez, C.P., Bizot, M., Gheeraert, C., Firmin, F., Ploton, M., Kretova, M., Palierne, G., Staels, B., et al. (2017). Inactivation of the nuclear orphan receptor COUP-TFII by small chemicals. ACS Chem. Biol. *12*, 654–663. https://doi.org/10.1021/acschembio.6b00593.

Lee, S.-Y., Kim, J.R., Hu, Y., Khan, R., Kim, S.-J., Bharadwaj, K.G., Davidson, M.M., Choi, C.-S., Shin, K.-O., Lee, Y.-M., et al. (2012a). Cardiomyocyte specific deficiency of serine palmitoyltransferase subunit 2 reduces ceramide but leads to cardiac dysfunction. J. Biol. Chem. *287*, 18429–18439. https://doi.org/10.1074/jbc.M111.296947.

Lee, Y.J., Huang, X., Kropat, J., Henras, A., Merchant, S.S., Dickson, R.C., and Chanfreau, G.F. (2012b). Sphingolipid signaling mediates iron toxicity. Cell Metab. *16*, 90–96. https://doi.org/10.1016/j.cmet.2012.06.004.

Levin, A.A., Sturzenbecker, L.J., Kazmer, S., Bosakowski, T., Huselton, C., Allenby, G., Speck, J., Kratzeisen, C., Rosenberger, M., Lovey, A., and Grippo, J.F. (1992). 9-cis retinoic acid stereoisomer binds and activates the nuclear receptor RXR alpha. Nature *355*, 359–361. https://doi.org/10.1038/355359a0.

Li, Z., Li, Y., Chakraborty, M., Fan, Y., Bui, H.H., Peake, D.A., Kuo, M.S., Xiao, X., Cao, G., and Jiang, X.C. (2009). Liver-specific deficiency of serine palmitoyltransferase subunit 2 decreases plasma sphingomyelin and increases apolipoprotein E levels. J. Biol. Chem. *284*, 27010–27019. https://doi.org/10.1074/jbc.M109.042028.

Lian, X., Zhang, J., Azarin, S.M., Zhu, K., Hazeltine, L.B., Bao, X., Hsiao, C., Kamp, T.J., and Palecek, S.P. (2013). Directed cardiomyocyte differentiation from human pluripotent stem cells by modulating Wnt/beta-catenin signaling under fully defined conditions. Nat. Protoc. *8*, 162–175. https://doi.org/10.1038/nprot.2012.150.

Lifton, R.P., Dluhy, R.G., Powers, M., Rich, G.M., Cook, S., Ulick, S., and Lalouel, J.M. (1992). A chimaeric 11 beta-hydroxylase/aldosterone synthase gene causes glucocorticoid-remediable aldosteronism and human hypertension. Nature *355*, 262–265. https://doi.org/10.1038/355262a0.

Lin, F.J., Chen, X., Qin, J., Hong, Y.K., Tsai, M.J., and Tsai, S.Y. (2010). Direct transcriptional regulation of neuropilin-2 by COUP-TFII modulates multiple steps in murine lymphatic vessel development. J. Clin. Invest. *120*, 1694–1707. https://doi.org/10.1172/JCI40101.

Lo, M.C., Aulabaugh, A., Jin, G., Cowling, R., Bard, J., Malamas, M., and Ellestad, G. (2004). Evaluation of fluorescence-based thermal shift assays for hit identification in drug discovery. Anal. Biochem. *332*, 153–159. https://doi.org/10.1016/j.ab.2004.04.031.

Lone, M.A., Hu€lsmeier, A.J., Saied, E.M., Karsai, G., Arenz, C., von Eckardstein, A., and Hornemann, T. (2020). Subunit composition of the mammalian serine-palmitoyltransferase defines the spectrum of straight and methyl-branched long-chain bases. Proc. Natl. Acad. Sci. USA *117*, 15591–15598. https://doi.org/10.1073/pnas.2002391117.

Luecken, M.D., and Theis, F.J. (2019). Current best practices in single-cell RNA-seq analysis: a tutorial. Mol. Syst. Biol. *15*, e8746. https://doi.org/10.15252/msb.20188746.

Makishima, M., Okamoto, A.Y., Repa, J.J., Tu, H., Learned, R.M., Luk, A., Hull, M.V., Lustig, K.D., Mangelsdorf, D.J., and Shan, B. (1999). Identification of a nuclear receptor for bile acids. Science *284*, 1362–1365.

Maurange, C., Cheng, L., and Gould, A.P. (2008). Temporal transcription factors and their targets schedule the end of neural proliferation in Drosophila. Cell *133*, 891–902. https://doi.org/10.1016/j.cell.2008.03.034.

Merrill, A.H., Jr. (2011). Sphingolipid and glycosphingolipid metabolic pathways in the era of sphingolipidomics. Chem. Rev. *111*, 6387–6422. https://doi.org/10.1021/cr2002917.

Merrill, A.H., Jr., Wang, E., and Mullins, R.E. (1988). Kinetics of long-chain (sphingoid) base biosynthesis in intact LM cells: effects of varying the extracellular concentrations of serine and fatty acid precursors of this pathway. Biochemistry *27*, 340–345.

Mettler, U., Vogler, G., and Urban, J. (2006). Timing of identity: spatiotemporal regulation of hunchback in neuroblast lineages of Drosophila by seven-up and Prospero. Development *133*, 429–437. https://doi.org/10.1242/dev.02229.

Miyake, Y., Kozutsumi, Y., Nakamura, S., Fujita, T., and Kawasaki, T. (1995). Serine palmitoyltransferase is the primary target of a sphingosine-like immunosuppressant, ISP-1/myriocin. Biochem. Biophys. Res. Commun. *211*, 396–403. https://doi.org/10.1006/bbrc.1995.1827.

Mlodzik, M., Hiromi, Y., Weber, U., Goodman, C.S., and Rubin, G.M. (1990). The Drosophila seven-up gene, a member of the steroid receptor gene superfamily, controls photoreceptor cell fates. Cell *60*, 211–224.

Molina, M.R., and Cripps, R.M. (2001). Ostia, the inflow tracts of the Drosophila heart, develop from a genetically distinct subset of cardial cells. Mech. Dev. *109*, 51–59.

Montemayor, C., Montemayor, O.A., Ridgeway, A., Lin, F., Wheeler, D.A., Pletcher, S.D., and Pereira, F.A. (2010). Genome-wide analysis of binding sites and direct target genes of the orphan nuclear receptor NR2F1/COUP-TFI. PLoS One *5*, e8910. https://doi.org/10.1371/journal.pone.0008910.

Moon, K.R., van Dijk, D., Wang, Z., Gigante, S., Burkhardt, D.B., Chen, W.S., Yim, K., Elzen, A.V.D., Hirn, M.J., Coifman, R.R., et al. (2019). Visualizing structure and transitions in high-dimensional biological data. Nat. Biotechnol. *37*, 1482–1492. https://doi.org/10.1038/s41587-019-0336-3.

Mwinyi, J., Bostro¨ m, A., Fehrer, I., Othman, A., Waeber, G., Marti-Soler, H., Vollenweider, P., Marques-Vidal, P., Schio¨ th, H.B., von Eckardstein, A., and Hornemann, T. (2017). Plasma 1-deoxysphingolipids are early predictors of

incident type 2 diabetes mellitus. PLoS One *12*, e0175776. https://doi.org/10.1371/journal.pone.0175776.

Narayanaswamy, P., Shinde, S., Sulc, R., Kraut, R., Staples, G., Thiam, C.H., Grimm, R., Sellergren, B., Torta, F., and Wenk, M.R. (2014). Lipidomic "deep profiling": an enhanced workflow to reveal new molecular species of signaling lipids. Anal. Chem. *86*, 3043–3047. https://doi.org/10.1021/ac4039652.

Osafune, K., Caron, L., Borowiak, M., Martinez, R.J., Fitz-Gerald, C.S., Sato, Y., Cowan, C.A., Chien, K.R., and Melton, D.A. (2008). Marked differences in differentiation propensity among human embryonic stem cell lines. Nat. Biotechnol. *26*, 313–315. https://doi.org/10.1038/nbt1383.

Othman, A., Saely, C.H., Muendlein, A., Vonbank, A., Drexel, H., von Eckardstein, A., and Hornemann, T. (2015). Plasma 1-deoxysphingolipids are predictive biomarkers for type 2 diabetes mellitus. BMJ Open Diabetes Res. Care *3*, e000073. https://doi.org/10.1136/bmjdrc-2014-000073.

Palanker, L., Necakov, A.S., Sampson, H.M., Ni, R., Hu, C., Thummel, C.S., and Krause, H.M. (2006). Dynamic regulation of Drosophila nuclear receptor activity in vivo. Development *133*, 3549–3562. https://doi.org/10.1242/dev.02512.

Parks, D.J., Blanchard, S.G., Bledsoe, R.K., Chandra, G., Consler, T.G., Kliewer, S.A., Stimmel, J.B., Willson, T.M., Zavacki, A.M., Moore, D.D., and Lehmann, J.M. (1999). Bile acids: natural ligands for an orphan nuclear receptor. Science *284*, 1365–1368.

Penno, A., Reilly, M.M., Houlden, H., Laura´ , M., Rentsch, K., Niederkofler, V., Stoeckli, E.T., Nicholson, G., Eichler, F., Brown, R.H., Jr., et al. (2010). Hereditary sensory neuropathy type 1 is caused by the accumulation of two neurotoxic sphingolipids. J. Biol. Chem. *285*, 11178–11187. https://doi.org/10.1074/jbc.M109.092973.

Pereira, F.A., Qiu, Y., Zhou, G., Tsai, M.J., and Tsai, S.Y. (1999). The orphan nuclear receptor COUP-TFII is required for angiogenesis and heart development. Genes Dev. *13*, 1037–1049.

Petersen, S.C., Watson, J.D., Richmond, J.E., Sarov, M., Walthall, W.W., and Miller, D.M., 3rd. (2011). A transcriptional program promotes remodeling of GABAergic synapses in Caenorhabditis elegans. J. Neurosci. *31*, 15362–15375. https://doi.org/10.1523/JNEUROSCI.3181-11.2011.

Petkovich, M., Brand, N.J., Krust, A., and Chambon, P. (1987). A human retinoic acid receptor which belongs to the family of nuclear receptors. Nature *330*, 444–450. https://doi.org/10.1038/330444a0.

Pipao´ n, C., Tsai, S.Y., and Tsai, M.J. (1999). COUP-TF upregulates NGFI-A gene expression through an Sp1 binding site. Mol. Cell. Biol. *19*, 2734–2745.

Ponzielli, R., Astier, M., Chartier, A., Gallet, A., The´ rond, P., and Se´ me´ riva, M. (2002). Heart tube patterning in Drosophila requires integration of axial and segmental information provided by the bithorax Complex genes and hedgehog signaling. Development *129*, 4509–4521.

Qiu, Y., Cooney, A.J., Kuratani, S., DeMayo, F.J., Tsai, S.Y., and Tsai, M.J. (1994). Spatiotemporal expression patterns of chicken ovalbumin upstream promoter-transcription factors in the developing mouse central nervous system: evidence for a role in segmental patterning of the diencephalon. Proc. Natl. Acad. Sci. USA *91*, 4451–4455.

Qiu, Y., Pereira, F.A., DeMayo, F.J., Lydon, J.P., Tsai, S.Y., and Tsai, M.J. (1997). Null mutation of mCOUP-TFI results in defects in morphogenesis of the glossopharyngeal ganglion, axonal projection, and arborization. Genes Dev. *11*, 1925–1937.

Renier, N., Wu, Z., Simon, D.J., Yang, J., Ariel, P., and Tessier-Lavigne, M. (2014). iDISCO: a simple, rapid method to immunolabel large tissue samples for volume imaging. Cell *159*, 896–910. https://doi.org/10.1016/j.cell.2014.10.010.

Revankar, C.M., Cimino, D.F., Sklar, L.A., Arterburn, J.B., and Prossnitz, E.R. (2005). A transmembrane intracellular estrogen receptor mediates rapid cell signaling. Science *307*, 1625–1630. https://doi.org/10.1126/science.1106943.

Rotthier, A., Auer-Grumbach, M., Janssens, K., Baets, J., Penno, A., Almeida-Souza, L., Van Hoof, K., Jacobs, A., De Vriendt, E., Schlotter-Weigel, B., et al. (2010). Mutations in the SPTLC2 subunit of serine palmitoyltransferase cause hereditary sensory and autonomic neuropathy type I. Am. J. Hum. Genet. *87*, 513–522. https://doi.org/10.1016/j.ajhg.2010.09.010.

Russo, S.B., Tidhar, R., Futerman, A.H., and Cowart, L.A. (2013). Myristate-derived d16:0 sphingolipids constitute a cardiac sphingolipid pool with distinct synthetic routes and functional properties. J. Biol. Chem. *288*, 13397–13409. https://doi.org/10.1074/jbc.M112.428185.

Saied, E., M., and Arenz, C. (2020). Synthesis and characterization of novel atypical sphingoid bases. ChemRxiv. https://doi.org/10.26434/chemrxiv.12094041.v1.

Saied, E.M., and Arenz, C. (2021). Stereoselective synthesis of novel sphingoid bases utilized for exploring the secrets of sphinx. Int. J. Mol. Sci. *22*, 8171.

Saied, E.M., Le, T.L., Hornemann, T., and Arenz, C. (2018). Synthesis and characterization of some atypical sphingoid bases. Bioorg. Med. Chem. *26*, 4047–4057. https://doi.org/10.1016/j.bmc.2018.06.031.

Saito, K., Chang, Y.F., Horikawa, K., Hatsugai, N., Higuchi, Y., Hashida, M., Yoshida, Y., Matsuda, T., Arai, Y., and Nagai, T. (2012). Luminescent proteins for high-speed single-cell and whole-body imaging. Nat. Commun. *3*, 1262. https://doi.org/10.1038/ncomms2248.

Sanjana, N.E., Shalem, O., and Zhang, F. (2014). Improved vectors and genome-wide libraries for CRISPR screening. Nat. Methods *11*, 783–784. https://doi.org/10.1038/nmeth.3047.

Santori, F.R., Huang, P., van de Pavert, S.A., Douglass, E.F., Jr., Leaver, D.J., Haubrich, B.A., Keber, R., Lorbek, G., Konijn, T., Rosales, B.N., et al. (2015). Identification of natural RORgamma ligands that regulate the development of lymphoid cells. Cell Metab. *21*, 286–298. https://doi.org/10.1016/j.cmet.2015.01.004.

Sasaki, H., Arai, H., Cocco, M.J., and White, S.H. (2009). pH dependence of sphingosine aggregation. Biophys. J. *96*, 2727–2733. https://doi.org/10.1016/j.bpj.2008.12.3926.

Sayin, S.I., Wahlstro¨ m, A., Felin, J., Ja€ntti, S., Marschall, H.U., Bamberg, K., Angelin, B., Hyo¨ tyla€inen, T., Ore sic , M., and Ba€ckhed, F. (2013). Gut microbiota regulates bile acid metabolism by reducing the levels of tauro-beta-muricholic acid, a naturally occurring FXR antagonist. Cell Metab. *17*, 225–235. https://doi.org/10.1016/j.cmet.2013.01.003.

Schwach, V., Verkerk, A.O., Mol, M., Monshouwer-Kloots, J.J., Devalla, H.D., Orlova, V.V., Anastassiadis, K., Mummery, C.L., Davis, R.P., and Passier, R. (2017). A COUP-TFII human embryonic stem cell reporter line to identify and select atrial cardiomyocytes. Stem Cell Rep. *9*, 1765–1779. https://doi.org/10.1016/j.stemcr.2017.10.024.

Shakoury-Elizeh, M., Protchenko, O., Berger, A., Cox, J., Gable, K., Dunn, T.M., Prinz, W.A., Bard, M., and Philpott, C.C. (2010). Metabolic response to iron deficiency in Saccharomyces cerevisiae. J. Biol. Chem. *285*, 14823–14833. https://doi.org/10.1074/jbc.M109.091710.

Shalem, O., Sanjana, N.E., Hartenian, E., Shi, X., Scott, D.A., Mikkelson, T.S., Heckl, D., Ebert, B.L., Root, D.E., Doench, J.G., and Zhang, F. (2014). Genome-scale CRISPR-Cas9 knockout screening in human cells. Science *343*, 84–87. https://doi.org/10.1126/science.1247005.

Shan, G., and Walthall, W.W. (2008). Copulation in C. elegans males requires a nuclear hormone receptor. Dev. Biol. *322*, 11–20. https://doi.org/10.1016/j.ydbio.2008.06.034.

Smith, C.A., Want, E.J., O'Maille, G., Abagyan, R., and Siuzdak, G. (2006). XCMS: processing mass spectrometry data for metabolite profiling using nonlinear peak alignment, matching, and identification. Anal. Chem. *78*, 779–787. https://doi.org/10.1021/ac051437y.

Srinivasan, R.S., Dillard, M.E., Lagutin, O.V., Lin, F.J., Tsai, S., Tsai, M.J., Samokhvalov, I.M., and Oliver, G. (2007). Lineage tracing demonstrates the venous origin of the mammalian lymphatic vasculature. Genes Dev. *21*, 2422–2432. https://doi.org/10.1101/gad.1588407.

Srinivasan, R.S., Geng, X., Yang, Y., Wang, Y., Mukatira, S., Studer, M., Porto, M.P., Lagutin, O., and Oliver, G. (2010). The nuclear hormone receptor Coup-TFII is required for the initiation and early maintenance of Prox1 expression in lymphatic endothelial cells. Genes Dev. *24*, 696–707. https://doi.org/10.1101/gad.1859310.

Srinivasan, R.S., and Oliver, G. (2011). Prox1 dosage controls the number of lymphatic endothelial cell progenitors and the formation of the lymphovenous valves. Genes Dev. *25*, 2187–2197. https://doi.org/10.1101/gad.16974811.

Starkey, N.J.E., Li, Y., Drenkhahn-Weinaug, S.K., Liu, J., and Lubahn, D.B. (2018). 27-Hydroxycholesterol is an estrogen receptor beta-selective negative allosteric modifier of 17beta-estradiol binding. Endocrinology *159*, 1972–1981. https://doi.org/10.1210/en.2018-00081.

Stehling, O., Mascarenhas, J., Vashisht, A.A., Sheftel, A.D., Niggemeyer, B., Ro¨ sser, R., Pierik, A.J., Wohlschlegel, J.A., and Lill, R. (2013). Human CIA2A-FAM96A and CIA2B-FAM96B integrate iron homeostasis and maturation of different subsets of cytosolic-nuclear iron-sulfur proteins. Cell Metab. *18*, 187–198. https://doi.org/10.1016/j.cmet.2013.06.015.

Steiner, R., Saied, E.M., Othman, A., Arenz, C., Maccarone, A.T., Poad, B.L., Blanksby, S.J., von Eckardstein, A., and Hornemann, T. (2016). Elucidating the chemical structure of native 1-deoxysphingosine. J. Lipid Res. *57*, 1194–1203. https://doi.org/10.1194/jlr.M067033.

Takamoto, N., You, L.R., Moses, K., Chiang, C., Zimmer, W.E., Schwartz, R.J., DeMayo, F.J., Tsai, M.J., and Tsai, S.Y. (2005). COUP-TFII is essential for radial and anteroposterior patterning of the stomach. Development *132*, 2179–2189. https://doi.org/10.1242/dev.01808.

Tang, K., Xie, X., Park, J.I., Jamrich, M., Tsai, S., and Tsai, M.J. (2010). COUP-TFs regulate eye development by controlling factors essential for optic vesicle morphogenesis. Development *137*, 725–734. https://doi.org/10.1242/dev.040568.

Tao, L.J., Seo, D.E., Jackson, B., Ivanova, N.B., and Santori, F.R. (2020). Nuclear hormone receptors and their ligands: metabolites in control of transcription. Cells *9*, 2606. https://doi.org/10.3390/cells9122606.

Tsai, S.Y., and Tsai, M.J. (1997). Chick ovalbumin upstream promoter-transcription factors (COUP-TFs): coming of age. Endocr. Rev. *18*, 229–240. https://doi.org/10.1210/edrv.18.2.0294.

Uhle´ n, M., Fagerberg, L., Hallstro¨ m, B.M., Lindskog, C., Oksvold, P., Mardinoglu, A., Sivertsson, A˚ ., Kampf, C., Sjo¨ stedt, E., Asplund, A., et al. (2015). Proteomics. Tissue-based map of the human proteome. Science *347*, 1260419. https://doi.org/10.1126/science.1260419.

Uhlen, M., Oksvold, P., Fagerberg, L., Lundberg, E., Jonasson, K., Forsberg, M., Zwahlen, M., Kampf, C., Wester, K., Hober, S., et al. (2010). Towards a knowledge-based Human Protein Atlas. Nat. Biotechnol. *28*, 1248–1250. https://doi.org/10.1038/nbt1210-1248.

Urs, A.N., Dammer, E., and Sewer, M.B. (2006). Sphingosine regulates the transcription of CYP17 by binding to steroidogenic factor-1. Endocrinology *147*, 5249–5258. https://doi.org/10.1210/en.2006-0355.

van Westen, G.J., Gaulton, A., and Overington, J.P. (2014). Chemical, target, and bioactive properties of allosteric modulation. PLoS Comput. Biol. *10*, e1003559. https://doi.org/10.1371/journal.pcbi.1003559.

Walker, A.K., Jacobs, R.L., Watts, J.L., Rottiers, V., Jiang, K., Finnegan, D.M., Shioda, T., Hansen, M., Yang, F., Niebergall, L.J., et al. (2011). A conserved SREBP-1/phosphatidylcholine feedback circuit regulates lipogenesis in metazoans. Cell *147*, 840–852. https://doi.org/10.1016/j.cell.2011.09.045.

Wang, Y., Nakayama, M., Pitulescu, M.E., Schmidt, T.S., Bochenek, M.L., Sakakibara, A., Adams, S., Davy, A., Deutsch, U., Lu€thi, U., et al. (2010). Ephrin-B2 controls VEGF-induced angiogenesis and lymphangiogenesis. Nature *465*, 483–486. https://doi.org/10.1038/nature09002.

Wang, Z., Gearhart, M.D., Lee, Y.W., Kumar, I., Ramazanov, B., Zhang, Y., Hernandez, C., Lu, A.Y., Neuenkirchen, N., Deng, J., et al. (2018). A non-canonical BCOR-PRC1.1 complex represses differentiation programs in human ESCs. Cell Stem Cell *22*, 235–251.e9. https://doi.org/10.1016/j.stem.2017.12.002.

Wang, Z., Oron, E., Nelson, B., Razis, S., and Ivanova, N. (2012). Distinct lineage specification roles for NANOG, OCT4, and SOX2 in human embryonic stem cells. Cell Stem Cell *10*, 440–454. https://doi.org/10.1016/j.stem.2012.02.016.

Wang, Z., Zhang, Y., Lee, Y.W., and Ivanova, N.B. (2019). Combining CRISPR/Cas9-mediated knockout with genetic complementation for in-depth mechanistic studies in human ES cells. BioTechniques *66*, 23–27. https://doi.org/10.2144/btn-2018-0115.

Wolf, F.A., Angerer, P., and Theis, F.J. (2018). SCANPY: large-scale single-cell gene expression data analysis. Genome Biol. *19*, 15. https://doi.org/10.1186/s13059-017-1382-0.

Wu, S.P., Cheng, C.M., Lanz, R.B., Wang, T., Respress, J.L., Ather, S., Chen, W., Tsai, S.J., Wehrens, X.H., Tsai, M.-J., and Tsai, S.Y. (2013). Atrial identity is determined by a COUP-TFII regulatory network. Dev. Cell *25*, 417–426. https://doi.org/10.1016/j.devcel.2013.04.017.

Yamaguchi, H., Zhou, C., Lin, S.C., Durand, B., Tsai, S.Y., and Tsai, M.J. (2004). The nuclear orphan receptor COUP-TFI is important for differentiation of oligodendrocytes. Dev. Biol. *266*, 238–251.

You, L.R., Lin, F.J., Lee, C.T., DeMayo, F.J., Tsai, M.J., and Tsai, S.Y. (2005). Suppression of Notch signalling by the COUP-TFII transcription factor regulates vein identity. Nature *435*, 98–104. https://doi.org/10.1038/nature03511.

Zelhof, A.C., Yao, T.P., Chen, J.D., Evans, R.M., and McKeown, M. (1995). Seven-up inhibits ultraspiracle-based signaling pathways in vitro and in vivo. Mol. Cell. Biol. *15*, 6736–6745.

STAR+METHODS

KEY RESOURCES TABLE

Reagent or resource	Source	Identifier
Antibodies		
InVivoMab anti-mouse CD16/CD32	Bio Cell	Cat#EB0307; RRID: AB_2736987
Anti-CD31 (rat clone ER-MP12)	Thermo Fisher	Cat#MA1-40074; RRID: AB_1072120
Anti-FLAG Alexa fluor 647 Mab (L5)	Thermo Fisher	Cat#MA1-142-A647; RRID: AB_2610655
Anti-FLAG FITC	Sigma-Aldrich	Cat#F4049; RRID: AB_439701
Anti-FLAG M2 magnetic beads	Sigma-Aldrich	Cat#M8823; RRID: AB_2637089
Anti-H3K27ac	Abcam	Cat#Ab4729; RRID: AB_2118291
Anti-human Cardiac Troponin T clone 13-11 alexa 647	BD Biosciences	Cat# 565744; RRID: AB_2739341
Anti-Human COUP-TFI/NR2F1 Clone H8132	R&D systems	Cat# PP-H8132-00; RRID: AB_2155493
Anti-Human COUP-TFII/NR2F2 Clone H7147	Perseus Proteomics	Cat# PP-H7147-00; RRID: AB_2314222
Anti-mouse Lyve1 monoclonal antibody (ALY7) biotin	Thermo Fisher	Cat# 13-0443-82; RRID: AB_1724157
Anti-mouse Lyve1 monoclonal antibody (ALY7) alexa 488	eBioscience	Cat#53-0443-82; RRID: AB_1633415
MECA-79, Alexa Fluor 488	Thermo Fisher	Cat# 53-6036-82; RRID: AB_10804391
Anti-Myc-tag	Millipore Sigma	Cat#05-724; RRID: AB_11211891
Anti-Prox1 (goat)	R&D technologies	Cat#AF2727; RRID: AB_2170716
Prox1 antibody AF405/AF647	Novus Biologicals	NBP1-30045; RRID: AB_1968604
Anti-TUBULIN	Sigma-Aldrich	Cat#T6074; RRID: AB_477582
Donkey anti-mouse Alexa 555	Thermo Fisher	Cat#A-31570; RRID: AB_2536180
Donkey anti-rabbit Alexa 555	Thermo Fisher	Cat#A-31572; RRID: 162543
Donkey anti-rat Alexa 790	Jackson Immunoresearch	Cat#712-655-153; RRID: AB_2340701
Donkey anti-mouse Alexa 594	Invitrogen	Cat# A21203; RRID: AB_2535789
Donkey anti-goat Alexa 647	Thermo Fisher	Cat#A-21447; RRID: AB_2535864
Goat anti-mouse IgG2a Alexa 488	Thermo Fisher	Cat#A-21131; RRID: AB_2535771
Goat anti-mouse Alexa Fluor 568	Thermo Fisher	Cat# A-11004; RRID: AB_2534072
Goat anti-Rabbit IgG-Peroxidase	Jackson Immunoresearch Lab	Cat#111-036-045; RRID: AB_2337943
Rabbit anti-Goat IgG-Peroxidase	Jackson Immunoresearch Lab	Cat#305-036-045; RRID: AB_2339409
Rabbit anti-Mouse IgG-Peroxidase	Jackson Immunoresearch Lab	Cat#315-036-045; RRID: AB_2340072
Bacterial strains		
One Shot Top10 chemically competent *E. coli*	Thermo Fisher	Cat#C404010
Stbl2 chemically competent *E. coli*	Thermo Fisher	Cat#10268019
T7 Express chemically competent *E.coli*	New England Biolabs	Cat#C2566H
Chemicals, peptides, and recombinant proteins		
1,3-Diaminopropane	Acros organics	Cat#112352500
10-nitrooleate	Cayman Chemicals	Cat#10008043
16:0 Lyso PE	Avanti Polar Lipids	Cat#856705
18:1(2S-OH) Ceramide	Avanti Polar Lipids	Cat#860828
1-deoxysphinganine	Avanti Polar Lipids	Cat#860493
1-deoxysphingosine	Avanti Polar Lipids	Cat#860470
1-deoxysphingosine (14Z)	Steiner et al., 2016	Saied E and Arenz, C
1-deoxysphingosine 14Z-d	Saied E and Arenz, C	Saied E and Arenz, C
1-deoxysphingosine-14Z-NBD	Saied E and Arenz, C	Saied E and Arenz, C
1-deoxysphingosine (6E)	Steiner et al., 2016	Saied E and Arenz, C
1-deoxysphingsoine (12E)	Steiner et al., 2016	Saied E and Arenz, C

(*Continued on next page*)

Continued

Reagent or resource	Source	Identifier
1-deoxysphingosine (13E)	Steiner et al., 2016	Saied E and Arenz, C
1-deoxysphingosine (8E)	Steiner et al., 2016	Saied E and Arenz, C
1-deoxysphinganine-4E,14Z-diene	Steiner et al., 2016	Saied E and Arenz, C
1-deoxysphingosine (4E)	Steiner et al., 2016	Saied E and Arenz, C
1-deoxysphingosine (14Z)	Steiner et al., 2016	Saied E and Arenz, C
1-deoxysphingosine (14E)	Steiner et al., 2016	Saied E and Arenz, C
1-desoxymethylsphingosine	Avanti Polar Lipids	Cat#860477
1-Methyl-L-Histidine	Sigma-Aldrich	Cat#67520
3- hydroxy-DL-Kynurenine	Sigma-Aldrich	Cat#H1771
4- Hydroxytamoxifen	Sigma-Aldrich	Cat# H6278
4E,14Z-Sphingadiene	Avanti Polar Lipids	Cat#860665
4E,8Z-Sphingadiene	Avanti Polar Lipids	Cat#860667
5- methyltetrahydrofolic acid	Cayman Chemicals	Cat#16159
6- hydroxy-melatonin	Cayman Chemicals	Cat#21857
7,8-dihydro-L-Biopterin	Cayman Chemicals	Cat#81882
7- dehydrocholesterol	Sigma-Aldrich	Cat#30800
9-cis retinoic acid	Cayman Chemicals	Cat#14587
9-nitrooleate	Cayman Chemicals	Cat#10008042
AFMK	Cayman Chemicals	Cat#10005254
all-trans-retinoic acid	Cayman Chemicals	Cat#11017
all-trans-5,6-epoxy retinoic acid	Santa Cruz	Cat#sc-210777
all-trans-retinal	Cayman Chemicals	Cat#18449
all-trans-retinol	Cayman Chemicals	Cat#20241
aminoacetone HCL	Cayman Chemicals	Cat#17573
anthranilic acid	Sigma-Aldrich	Cat#A89855
C16 ceramide (d18:1/16:0)	Avanti Polar Lipids	Cat#860516
C16 dihydroceramide (d18:0/16:0)	Avanti Polar Lipids	Cat#860634
C17 ceramide (d18:1/17:0)	Avanti Polar Lipids	Cat#860517
C18:1 Dihydroceramide (d18:0/18:1(9Z))	Avanti Polar Lipids	Cat#860624
Cerebrosides	Avanti Polar Lipids	Cat#131303
D-erythro-Sphingosine (d18:1)	Avanti Polar Lipids	Cat#860490
Dopamine	Sigma-Aldrich	Cat#H8502
Dl-2-pyrrolidone-5-carboxylic acid	Acros	Cat#232930050
DL-Homocysteine	Sigma-Aldrich	Cat#H4628
Ganglioside GM1	Avanti Polar Lipids	Cat#860065
Homogentisic acid	Sigma-Aldrich	Cat#H0751
Kynurenine	Cayman Chemicals	Cat#11305
L-2-aminobutyric	Sigma-Aldrich	Cat#A2636
L-cystathionine	Sigma-Aldrich	Cat#C7505
L-cysteic acid	TCI	Cat#C0514
L-selenmethionine	Cayman Chemicals	Cat#16005
L-selenocystine	Cayman Chemicals	Cat#17793
L-sepiapterin	Cayman Chemicals	Cat#81650
L-threo-sphingosine (d18:1)	Avanti Polar Lipids	Cat#860489
Methylglyoxal	MP	Cat#155558
Myristic acid	Cayman Chemicals	Cat#13351
N-methyl-D-erythro-sphingosine	Avanti Polar Lipids	Cat#860495
N-arachidonoyl-3-hydroxy-g-aminobutyric acid	Cayman Chemicals	Cat#10158
N-butyryl-L-Homocysteine thiolactone	Cayman Chemicals	Cat#10011204
N-cis-tetradec-9Z-enoyl-L-homoserine lactone	Cayman Chemicals	Cat#10012672

(*Continued on next page*)

Continued

Reagent or resource	Source	Identifier
Neopterin	Cayman Chemicals	Cat#12057
N-oleyl-L- serine	Cayman Chemicals	Cat#13058
Octanoyl carnitine	Cayman Chemicals	Cat#15048
Phenylacetaldehyde	Alfa Aesar	Cat#A14263
Phytanic acid	Cayman Chemicals	Cat#90360
Phytol	Cayman Chemicals	Cat#17401
S-adenosyl-L-homocysteine	Sigma-Aldrich	Cat#A9384
S-desoxymethylsphinganine	Avanti Polar Lipids	Cat#792270
serine	Sigma-Aldrich	Cat#S-5511
Serotonin	Cayman Chemicals	Cat#14332
sodium mercaptopyruvate	Santa Cruz	Cat#sc-236908
succinic acid	acros	Cat#158751000
Sulfatides	Avanti Polar Lipids	Cat#131305
Taurine	Sigma-Aldrich	Cat#T8691
tetrahydro-l-biopterin	Cayman Chemicals	Cat#81880
trans-4-hydroxy-proline	Acros	Cat#121780100
Tryptamine HCL	Sigma-Aldrich	Cat#245557
70% ethanol	American Bio	Cat#AB04010-00500
cOmplete protease inhibitor cocktail	Roche	Cat#11873580001
DTT	American Bio	Cat#AB00490-00010
Hepes	American Bio	Cat#AB06021-00100
Imidazole	American Bio	Cat#288-32-4
isopropyl-b-D-thiogalactopyranoside (IPTG)	American Bio	Cat#AB00841
KCl	Sigma-Aldrich	Cat#P9541-500G
$MgCl_2$	American Bio	Cat#AB09006-00100
MS grade acetic acid	Sigma-Aldrich	Cat#A6283
MS grade methanol	Sigma-Aldrich	Cat#34860
MS grade acetonitrile	Thermo Fisher	Cat#TS-51101
NaCl	American Bio	Cat#AB01915-01000
NaN3	Sigma-Aldrich	Cat#S2002-200G
Paraformaldehyde	Electron Microscopy Sciences	Cat#15710
PhosSTOP protease inhibitor	Sigma-Aldrich	Cat#4906837001
PMSF	Sigma-Aldrich	Cat#329-98-6
Sunflower seed oil	Sigma-Aldrich	Cat#S5007
SYPRO Orange	Thermo Fisher	Cat#S6650
TCEP	Sigma-Aldrich	Cat#C4706-2G
Tris 1M Solution, pH 8.0	American Bio	Cat#AB14043-01000
Trizol	Thermo Fisher	Cat#AM9738
Water	American Bio	Cat#AB02128-00500
3xFLAG peptide	Sigma-Aldrich	Cat#F4799
FL-PGC1A peptide	Life technologies	Cat#PV4421
FL-SMRT ID1 peptide	Life technologies	Cat#PV4620
FL-SMRT ID2 peptide	Life technologies	Cat#PV4423
FL-SRC2-1 peptide	Life technologies	Cat#PV4584
FL-SRC2-2 peptide	Life technologies	Cat#PV4586
FL-SRC2-3 peptide	Life technologies	Cat#PV4588
ATCC Endothelial cell growth kit-VEGF	ATCC	Cat#PCS-100-041
ATCC Vascular Cell Basal Medium	ATCC	Cat#PCS-100-030
DMEM	Gibco	Cat#11965
DMEM-F12	Thermo Fisher	Cat#13320033

(*Continued on next page*)

Continued

Reagent or resource	Source	Identifier
Express Five SFM media	Gibco	Cat#10486025
Expi293 medium	Thermo Fisher	Cat#A1435101
FreeStyle F17 expression medium	Thermo Fisher	Cat#A1383502
KSR medium	Thermo Fisher	Cat#10828010
mTeSR1 media	Stem Cell Technologies	Cat#85850
OptiMEM media	Thermo Fisher	Cat#31985088
RPMI-1640	Gibco	Cat#11875-093
StemFlex medium	Thermo Fisher	Cat#A3349401
B-27	Thermo Fisher	Cat#17504044
BSA fatty acid free	Sigma-Aldrich	Cat#A6003
Fetal Bovine Serum	Sigma-Aldrich	Cat#F2442
glutamax	Thermo Fisher	Cat#35050061
L-Glutamine	Gibco	Cat#25030-081
Insulin-Transferrin-Selenium (ITS-A)	Thermo Fisher	Cat#51300044
Insulin-free B-27	Thermo Fisher	Cat#A1895601
N2 supplement	Thermo Fisher	Cat#17502001
Pen/strep	Gibco	Cat#15140-122
Matrigel	BD Biosciences	Cat#354277
Doxycycline	Sigma-Aldrich	Cat#D9891
4-hydroxytamoxifen	Sigma	Cat#H6278
Geneticin (G418)	Thermo Fisher	Cat#10131035
Hygromycin	Invitrogen	Cat#10687-010
Puromycin	Sigma-Aldrich	Cat#P8833
Blastocydin	Thermo Fisher	Cat#A1113902
Myriocin	Sigma-Aldrich	Cat#476300
4-Methoxy-1-Naphthol	Sigma-Aldrich	Cat#174556
Rock inhibitor Y-27632	Tocris	Cat#1254
IWP2	Tocris	Cat#3533
CHIR99021	Tocris	Cat#4423
Accutase	Stem Cell Technologies	Cat # 07920
Collagenase D	Sigma-Aldrich	Cat#11088882001
DNase I	Sigma-Aldrich	Cat#D4263
Dispase	Stem Cell Technologies	Cat#07913
TripLE-Express	Gibco	Cat#12605-010
lipofectamine 3000	Thermo Fisher	Cat#L3000015
Cellfectin II reagent	Invitrogen	Cat#10362100
Polyethyleneimine (PEI)	Polyscience	Cat#24765
4*Laemmli sample buffer	Bio-Rad	Cat#161-0747
Ca++ $MgCl_2^{++}$ containing DPBS	Gibco	Cat#14040-117
Elution buffer	Sigma-Aldrich	Cat#G4251
fixation/permeabilization buffer	Thermo Fisher	Cat#00-5523-00
HBS-P+ 10x	Fisher Scientific	Cat#50-105-5346
RIPA lysis and extraction buffer	Thermo Fisher	Cat#89900
TURBO DNA-free kit	Thermo Fisher	Cat#AM1907
Ribo-Zero Gold Kit (Human/Mouse/Rat probe)	Illumina	Cat#MRZH11124
NEBNext Ultra RNA Library Prep Kit	Illumina	Cat# E7770
Qubit 2.0 Fluorometer RNA assay	Invitrogen	Cat#Q32855
KAPA qPCR assay	KAPA Biosystems	Cat#KK4601
SuperScript II Reverse Transcriptase	Thermo Fisher	Cat#18064014
iTaq Universal SYBR Green Supermix	Bio-Rad	Cat#M7128

(*Continued on next page*)

Continued

Reagent or resource	Source	Identifier
GoTaq green master mix	Promega	Cat#M7128
precast SDS-PAGE gel	Bio-rad	456-1096
Immobilon transfer membranes	Merck	Cat#IPVH00010
Supersignal West Pico Chemiluminescent Substrate	Thermo Fisher	Cat#34580
Ni-NTA column	Qiagen	Cat#30250
Glutathione Sepharose-4B	GE Healthcare	Cat#17-0756-01
Critical commercial assays		
BD Cytofix/Cytoperm fixation/permeabilization kit	BD biosciences	Cat#554714
Bio-Rad Protein Assay Kit II	Bio-rad	Cat#5000002
dual luciferase reporter kit	Promega	Cat#E1960
KAPA Express Extract Kit	Kapa Biosystems	Cat#07961804001
HotStart mouse genotyping kit	Kapa Biosystems	KK7352
Neon Transfection system kit	Invitrogen	Cat#MPK10025
Deposited data		
Bulk RNA-seq	This paper	GEO: GSE184913
Single-cell RNA-seq	This paper	GEO: GSE185456
Experimental models: Cell lines		
HEK-293FT	Invitrogen	Cat#R70007 RRID: CVCL_6911
HEK-293FT$^{3xFLAG\ NR2F1\text{-}LBD}$	This paper	N/A
HEK-293FT$^{3xFLAG\ RAR\text{-}LBD}$	This paper	N/A
HEK-293FT$^{FASN\text{-}/\text{-}}$	This paper	N/A
HEK-293FT$^{PCYT1A\text{-}/\text{-}}$	This paper	N/A
HEK-293FT$^{PCYT1B\text{-}/\text{-}}$	This paper	N/A
Hela cells	Santori et al., 2015	N/A
Time Cells	ATCC	Cat#CRL-4025
S2	Santori et al., 2015	N/A
Human embryonic stem cells (hESCs) H9	WiCell Research Institute	hESC Line: WA09 RRID: CVCL_9773 C25661
NR2F2-KO hESC (H9)	This paper	Clone 45
NR2F1-NR2F2 DKO hESC (H9)	This paper	Clones 55 and 93
DKO^{HSAN} hESC (H9) Knockin	This paper	Clones 1 and 2
WT^{HSAN} hESC (H9) Knockin	This paper	Clones 1 and 2
Experimental models: Organisms and strains		
C57bl/6 Cdh5 CreERT2	Cancer Research UK	N/A
C57bl/6 Prox1 CreERT2	Cancer Research UK	N/A
Sptlc2$^{f/f\ tm2.1Jia}$	Li et al, 2009	N/A
Sptlc2$^{f/f\ Prox1\ CreERT2}$	This paper	N/A
Sptlc2$^{f/f\ Cdh5\ CreERT2}$	This paper	N/A
B6;129S7-Nr2f2$^{f/f\ tm2Tsa/Mmmh}$	MMRRC	Strain#032805-MU
Nr2f2$^{f/f\ Prox1\ CreERT2}$	This paper	N/A
Nr2f2$^{f/fCdh5\ CreERT2}$	This paper	N/A
Oligonucleotides		
Table S2 related to key resources table. Oligos.	This paper	N/A
Recombinant DNA		
The Renilla luciferase (RL) plasmid pRL-CMV	Promega	Cat#E2261
PGL4.31[luc2p/GAL4UAS/Hygro] (luc2p)	Promega	Cat#C935A
Lenticrispr Version 2 vector	Addgene	Cat#52961
pHM1-Gal4(UAS)	Santori et al., 2015	N/A

(*Continued on next page*)

Continued

Reagent or resource	Source	Identifier
pHM1 6xDR0A	This paper	N/A
pHM1 NGF1A	This paper	N/A
pNGF1A-nano	This paper	N/A
pHM1 6xDR0A to 6xDR6A	This paper	N/A
pHM1-IL17	This paper	N/A
pcDNA3.1 NR2F2 mutants	This paper	N/A
pluc2p-ffluc-CMV	This paper	N/A
pET45b(+) 6xHis-GST- NR2F1-LBD	This paper	N/A
pET45b(+) 6xHis-GST- NR2F2-LBD	This paper	N/A
pAc-NR2F6	This paper	N/A
pAC Gal4-DBD-svp-LBD	This paper	N/A
pAC Gal4-DBD-NR2F1-LBD	This paper	N/A
NR2F1	Open Biosystems	Cat#MMM1013-202739977
NR2F2	Open Biosystems	Cat#MMM1013-202769921
NR2F6	Open Biosystems	Cat#MMM1013-202762257
pcDNA3.1 Gal4-DBD-NR2F1-LBD	This paper	N/A
pcDNA3.1 6xHis-NR2F2-LBD	This paper	N/A
pcDNA3.1 3x-Flag NR2F1-LBD	This paper	N/A
pcDNA3.1 3x-Flag huRARA-LBD	This paper	N/A
pcDNA3.1	Invitrogen	Cat#V790-20
6xHis-NR2F6-LBD	This paper	N/A
6xHis-GST-NR2F1-LBD	This paper	N/A
6xHis-GST-NR2F2-LBD	This paper	N/A
pET45b(+) vector	Millipore Sigma	Cat#71327
pET45b(+) 6xHis-GST tag vector	This paper	N/A
Table S1 related to key resources table. cDNAs	This paper	N/A
Software		
Imaris version 9 software	Oxford Instruments	N/A
ImageJ software	NIH	https://imagej.nih.gov/ij/
Fiji software	ImageJ.net	N/A
Graphpad prism 5	Graphpad.com	N/A
FACS Diva	BD biosciences	N/A
FlowJo version 10	Flowjo	N/A
Leica LAS X	Leica	N/A
Olympus FV10 software	Olympus	N/A
XCMS package	Smith et al., 2006	N/A
Other		
Fluorescence polarization measurements black 96-well plates	Thermo Fisher	Cat#137101
Fluorescence polarization measurements black 384 well plates	Thermo Fisher	Cat#4511
Luciferase assays white 384 well plates	Thermo Fisher/corning	Cat#3574
Lab-TEK II chamber slides	Nunc	Cat#154941
Cell strainers	Fisherbrand	Cat#22363549
Steriflip-GP sterile centrifuge tube filter unit	Millipore Sigma	Cat#SCGP00525
Nickel NTA sensor chip (series S)	GE Healthcare	Cat#28-9949-51
Cytoflex flow cytometer	Beckman Coulter	N/A
LSRII	BD biosciences	N/A
Gene Pulser XcelI	Bio-Rad	N/A

(*Continued on next page*)

Continued		
Reagent or resource	Source	Identifier
Gene Pulser cuvette	Bio-Rad	N/A
Neon Transfection System	Invitrogen	N/A
CFX96 instrument qPCR & TS Assay	Bio-Rad	N/A
Leica S5 confocal microscope	Leica	N/A
Olympus FV1200 confocal microscope	Olympus	N/A
FEI Tecnai TEM	FEI	N/A
Morada CCD camera	Olympus	N/A
Ultramicroscope II	Miltenyi Biotec, Bieliefeld, Germany	N/A
Zeiss 880 microscope	Zeiss	N/A
FPLC system	Bio-Rad	Cat#780-1650
Spectramax M5 reader	Molecular Devices	N/A
Agilent 4200 TapeStation	Agilent Technologies, Palo Alto, CA, USA	N/A
Biacore T100 system	GE Healthcare, Atlanta, GA, USA	N/A
Biotek luciferase reader	Biotek	N/A
Envision luciferase reader	Perkin-Elmer	N/A

RESOURCE AVAILABILITY

Lead contact

Further information and requests for resources and reagents should be directed to and will be fulfilled by the Lead Contact, Fabio Santori (fabio.santori@yale.edu).

Material availability

All plasmids, reagents, and cell lines are available upon request. The *Prox1* and *Cdh5* CreERT2 mouse models require written permission from Cancer Research UK/Ximbio.

Data and code availability

Bulk-RNA-seq and single-cell RNA-seq data are available through NCBI GEO datasets: access numbers GSE184913 (bulk RNA-seq) and GSE185456 (single-cell RNA-seq).

This manuscript did not generate new code.

EXPERIMENTAL MODEL AND SUBJECT DETAILS

HEK-293FT and HeLa cells were grown in DMEM (Gibco) supplemented with 2 mM Glutamine, 10,000 units/mL Penicillin/Streptomycin, and 10 % FBS at 37°C and 5% CO_2. Cultures were passaged every 5-6 days by adding TrypLE (Gibco) and re-plating at 1:10 ratio.

Drosophila melanogaster S2 cells were maintained in Express Five SFM media (Gibco) at room temperature in the dark and passaged once a week.

Sptlc2 $^{tm2.1Jia}$ (Li et al., 2009), *Prox1*^{CreERT2} (Bazigou et al., 2011) and *Cdh5*^{CreERT2} (Wang et al., 2010) mice were obtained from the Cancer Research Consortium (UK) under an MTA. *Nr2f2*$^{f/f}$ mice were re-derived from frozen sperm (B6;129S7-*Nr2f2*$^{tm2Tsa/Mmmh}$) received from the Mutant Mouse Regional Resource Center (MMRRC) at the University of Missouri. Mice were maintained in the Yale Animal Resources TAC facility and used under the approved IACUC protocols.

H9 human embryonic stem cells (WA09, NIH approval number NIHhESC-10-0062) were grown in feeder-free conditions in plates coated with Matrigel (BD Biosciences) in E8 media (Thermo Fisher) or mTeSR1 media (Stem Cell Technologies) at 37°C and 5% CO_2. Cultures were passaged every 4 days by adding 1mg/mL Dispase (Stem Cell Technologies) for 5 min at 37°C and re-plating at a 1:10 ratio.

METHOD DETAILS

Insect and mammalian reporter systems

pGL4.31[luc2p/GAL4UAS/Hygro] vector (Promega) containing firefly luciferase under GAL4(UAS) transcriptional control was modified to replace the late SV40 promoter with the Drosophila melanogaster hsp70 promoter (Santori et al., 2015). This reporter (referred to as pHM1) was used in experiments with GAL4(DBD)-NHR(LBD) fusion proteins in insect cells.

GAL4(DBD)-NR2F1(LBD) and GAL4(DBD)-Svp(LBD) fusion proteins were cloned in insect expression vector pAc driven by the Drosophila melanogaster actin promoter (Huh et al., 2011).

Mammalian synthetic reporter plasmids for NR2F1 and NR2F2 receptors were constructed by replacing the GAL4 (UAS) sequence of pHM1 with six tandem repeats of the conserved AGGTCA NR2F binding site (AGGTCAAGGTCAAGGTCAAGGTCAAGGTC AAGGTCAAGGTCAAGGTCA) (pHM1 6xDR0A plasmid) (Montemayor et al., 2010; Pipao´n et al., 1999; Zelhof et al., 1995).

Native mammalian NR2F2 reporter used in Figures S1F, 2C, and S2C was constructed by replacing the GAL4 (UAS) sequence of pHM1 with a single NR2F2 binding site found in the NGF1A promoter (TCACGGCGGAGGCGGGCCCGGGTATATAA) (pHM1-NGF1A) (Pipao´n et al., 1999). Native NR2F2 mammalian reporter used in Figures 2C and S2C utilized a fluorescent-bioluminescent fusion of *Renilla* luciferase and Venus fluorescent protein nanolantern (pHM1-NGF1A-nano) (Saito et al., 2012) in place of the firefly luciferase.

The NR2F6 reporter was constructed using the NR2F6 bindings site found in the IL-17 promoter (AATGGAAAGTTTTCTGACCC ACTTTAAATC) (pHM1-IL17) (Hermann-Kleiter et al., 2012).

6x(DR0A-DR6A) reporters were constructed by replacing the GAL4 (UAS) sequence of pHM1 with synthetic oligos described in Table S1.

CMV-driven NHR expression plasmids were obtained from commercial sources (Table S1-Plasmids).

The *Renilla* luciferase (RL) plasmid pRL-CMV (Promega) was used for normalization in mammalian cells, RL under a Pol2 promoter (Huh et al., 2011) was used for normalization in insect cells. In experiments utilizing the nanolantern bioluminescent reporter (Figures 2C and S2C) normalization was performed with the filrefly luciferase expression plasmid pluc2p-ffluc-CMV (Promega).

Enzyme overexpression screening

We identified all known metabolic genes in the mouse and human genomes using data from the Mouse Genomics Informatics (MGI) and the Human Protein Atlas databases (Eppig, 2017; Uhlen et al., 2010). The resulting list contained 1336 enzymes and excluded protein kinases, phosphatases, DNA and RNA polymerases as well as enzymes involved in protein translation and modification. Enzymes with no known human homologues were removed from the list. The list was further filtered to select a set of 516 enzymes that represent rate limiting metabolic enzymes and enzymes involved in secondary metabolism (Key Resources Table S1-Metabolic Enzyme cDNA Clones). The cDNA clones were purchased from commercial suppliers and validated by sequencing.

For the screening, transfections were performed as described below (*Reporter assays in mammalian cells*) using the following DNA amounts: 20-100 pg of *Renilla* normalization plasmid, 5-10 ng of reporter plasmid, 10-20 ng of NHR plasmid and 10 ng of enzyme/empty vector per well. Expression of transfected proteins was tested for a subset of clones by WB with anti-FLAG antibody (Sigma).

Metabolite screening

Synthetic metabolites were purchased from suppliers indicated in Table S1-Reagents. Mammalian or insect cells were trans- fected with the appropriate NHR plasmids and reporters as described below (*Reporter assays in mammalian cells* and *Reporter assays in insect cells*). 24 h after transfection, synthetic metabolite diluted in the appropriate solvent at concentration of 5-10 mM was added. Reporter activity was measured 16 h after the addition of metabolite as relative luciferase unit (RLU) ratio to vehicle (solvent alone).

Preparation of sphingolipid–BSA complexes

In mammalian cells, the uptake of sphingolipids is greatly improved by conjugation to BSA (Penno et al., 2010). For staining and delivery of sphingolipids to live and fixed cells sphingolipid-BSA complexes were prepared as follows. Sphingolipids were dissolved in ethanol at 200 mM concentration. Fatty acid free BSA (Sigma) was dissolved in PBS pH7.4 supplemented with 10 mM Hepes pH7.4 at 20 mM concentration. A tube with 10 mL of BSA solution was placed on a vortex mixer and 200 mL sphingolipid stock solution was added while it was vortexing. This produces a complex of 20 mM BSA: 20 mM sphingolipid that can be stored at -20^{0}C.

For measurements of the sphingolipid uptake, cells were washed with serum-free medium and BSA-sphingolipid complexes were added at the desired concentration. Cells were incubated at 4°C for 30 min, washed several times with ice-cold medium, incubated at 37°C for 30–90 min and imaged. For tissue culture experiments the complexes were added directly to culture medium cells every time medium was changed.

Reporter assays in mammalian cells

Mammalian reporter assays were performed as previously described (Santori et al., 2015). One day prior to transfection, HEK-293FT cells were plated at density of 5 x 10^4 cells per well in flat bottom 96 well plates in regular growth medium. Before transfection, medium was replaced with antibiotic-free DMEM supplemented with 1 % FBS. DNA mix consisted of 20-100 pg of *Renilla* normalization plasmid, 5-10 ng of reporter plasmid and 10-20 ng of NHR plasmid per well of 96 well plate. The DNA was diluted in 10 ml of OptiMEM media (Thermo Fisher) supplemented with 60 mg/mL polyethyleneimine (PEI) (Polyscience) and, after 10 min incubation at RT, added to the well. Transfected cells were maintained at 37°C and 5% CO_2 for 24 h, medium was replaced for regular growth medium and cells cultured for another 24 h. Luciferase activity was detected using the dual luciferase reporter kit (Promega).

Reporter assays in insect cells

One day prior to transfection, S2 cells were plated at a density of 1.5 -2.5 x 10^5 cells per well in flat bottom 96 well plates in growth medium. DNA mixture consisted of 2-5 ng of *Renilla* normalization plasmid, 10-25 ng of reporter plasmid and 20-50 ng GAL4-NHR

fusion plasmid per well of 96 well plate. DNA was diluted in 75ml of growth media containing 0.5 ml of Cellfectin II (Invitrogen) and added to the cells. Cells were maintained for 48 h and luciferase activity was detected using the dual luciferase reporter kit (Promega).

Cell-based reporter assays for sphingolipids in mammalian cells

Assays were performed in HEK-293FT or Hela cells. Cells were transfected with synthetic or native reporter, appropriate NHR plasmid and a *Renilla* normalization plasmid as described above. Sphingolipid-BSA complexes were diluted in media containing 1% FBS and added to the transfected cells 24 h after transfection. Vehicle-BSA complexes were used as controls. Cells were main- tained for another 24 h and luciferase activity was detected using the dual luciferase reporter kit (Promega).

Immunoprecipitation and lipidomics

Stable clones of HEK-293FT cells expressing 3xFLAG-NR2F1(LBD) or 3xFLAG-RARA(LBD) were established as follows. LBDs were cloned into pcDNA3.1 vector (Invitrogen). 300 ng of plasmid were diluted in 300 ml of serum-free DMEM medium containing 60 mg/mL PEI. DNA-Reagent mixture was incubated for 10 min at room temperature and added to the cells growing in a well of 6 well plate. After hygromycin (Invitrogen) selection the resistant cells were cloned and screened for expression of FLAG-LBD protein by FACS with Anti-FLAG-Alexa Fluor 647 or anti-FLAG FITC antibodies at 1:200-1:400 dilutions. The selected clones were grown as high-density suspension cultures in Expi293 medium (Thermo Fisher) supplemented with 500 nM all-trans-retinoic acid at 37°C in 10% CO_2.

Nuclear extracts were prepared as follows. 1 x 10^8 cells were washed in PBS and resuspended in hypotonic buffer (20 nM Hepes pH 7.9, 1.5 mM MgCl, 10 mM KCl, 0.1 mM PMSF, 1 mM DTT, cOmplete protease inhibitor cocktail (Roche). The cells-to-buffer ratio was adjusted to 1 x 10^8 cells/mL and kept constant for the entire procedure. After 15-20 min incubation on ice, cells where homogenized 6-7 times with a Dounce homogenizer, transferred into Eppendorf tubes and centrifuged at 15,000 x g for 15 min. The pellet was resuspended in buffer containing 20 mM Hepes pH 7.9, 1.5 mM $MgCl_2$, 0.2 mM EDTA, 25 % Glycerol, 420 mM KCl, 0.1 mM PMSF, 1 mM DTT and protease inhibitor cocktail. The pellet was homogenized 7-8 times with a Dounce homogenizer and placed on rotator shaker at 4 °C for 1–2 h. After incubation, the extract was centrifuged for 30 min at 15,000 xg. Supernatant was transferred into a new tube and incubated with 40 ml of anti-FLAG M2 magnetic beads (Sigma) on rotator shaker for 1 h at 4°C. After incubation, beads were washed 4 times with buffer containing 50 mM Tris HCl pH 7.4, 100 mM NaCl and protease inhibitor cocktail. FLAG-LBDs were eluted by 30 min incubation with 150 ng/mL of 3xFLAG peptide (Sigma) at 4°C. An aliquot corresponding to 1/20 of the IP was analyzed by Western blotting to confirm the presence of FLAG-LBD.

The remaining IP material was processed following 2 treatment schemes - scheme 1 to isolate specifically hydrophobic ligands and scheme 2 to isolate ligands that are potentially hydrophilic. In the scheme 1, a lipid extraction was performed using 2:1 chloroform-methanol mixture following the Folch procedure (Folch et al., 1957). The organic phase was collected and dried under N_2 stream. Metabolite displacement experiments were performed with samples treated under scheme 1 by adding 5 mM of synthetic deuterated 1-deoxysphingosine-14Z-*d* (Saied and Arenz, 2020) to samples of both NR2F1-LBD and RARA-LBD during the immunoprecipitation procedure. The scheme 2 was used in general immunoprecipitation procedures to identify potential hydrophilic ligands bound to NR2F1-LBD but not RAR-LBD in C18+ and Hilic- modes, 3% MS grade acetic acid (Sigma) was added to the immunoprecipitates followed by addition of 40% MS grade methanol (Sigma) and 40% MS grade acetonitrile (Thermo Fisher) so that the ratio of of IP: MEOH:ACN is 20:40:40. This mixture was vortexed for 30 seconds and incubated overnight at -20^{0}C. The next day samples were centrifuged at 15,000 x g for 15 min at 4 °C. The supernatant was collected and vacuum-dried. The protein pellet was frozen for further analysis. The tubes containing the dried metabolites and protein pellets were maintained at -80 °C until processing.

3-5 IP repeats for each set of experimental conditions were processed simultaneously by LC-MS. We first tested whether we could identify masses corresponding to derivatives of all-trans-retinoic acid in RARA samples. We found a 14.76 fold enrichment of a [M+H-H2O]+ adduct of exact mass m/z 283.2059 and mean retention time 27.5459 corresponding to retinoic acid in RARA but not NR2F1 samples (p value 0.01) in C18+ mode. To identify all possible metabolites bound to NR2F1 LBD we scanned all samples by C18+ and Hilic negative modes. Negative mode analysis was performed using a Phenomenex Luna-NH2 column (1.0x150 mm, 100A, 3 mm) at the flowrate of 50 ml/min, mobile phase A= 20mM NH_4OAc/40 mM NH_4OH and mobile phase B=5:95 H_2O:ACN. The injection volume was 8 ml, gradient: T0: 0:100 T5:0:100 T45:100:0 T60:100:0, stop time= 60 min, 9 min post time to re-equilibrate the column. MS settings were: scanning m/z=70-1100, dry gas flowrate: 8L/min, nebulizer pressure 8 psi, dry gas temperature =325 ^{0}C. Positive mode analysis used a C18 1.0x150mm column at a flowrate of 50 ml/min, mobile phase A= H_2O/0.1% formic acid and mobile phase B=ACN/0.1% formic acid. The injection volume was 8 ml, gradient: T0: 95:5 T5:95:5 T50:5:95 T60:5:95 stop time= 61 min, 9 min post time to re-equilibrate the column. MS settings were: scanning m/z=70-1100, dry gas flowrate: 8L/min, nebulizer pressure 8 psi, dry gas temperature =325 ^{0}C, acquisition in positive mode. Final data from the LC-MS run was analyzed using XCMS package (Smith et al., 2006). After XCMS analysis that included alignment, elimination of isotypic peaks we selected our data search parameters: Fold change > 3, maximum intensity > 30–50000, p value < 0.05. The files were inspected manually to confirm and check for accuracy or adjust for missing peaks.

Sphingolipidome of TIME cells

Cells were harvested, counted, and washed twice with PBS pH7.4. The nuclear extract was prepared by resuspending the cell pellet after the last wash with1 mL lysis buffer (10 mM Hepes pH7.6, 10 mM KCl, 1.5 mM MgCl2, 5% Glycerol, 0.2 mM PMSF, 1 mM DTT and cOmplete protease inhibitor cocktail (Roche)) and incubated on ice for 7-20 min. Cells were vortexed and spun at 21000 xg for 10 min at 4°C. The supernatant is the cytosol. The pellet (nuclear fraction) was washed twice in lysis buffer at 21000 xg for 10 min at

4°C. The final pellet was resuspended in 1 mL lysis buffer. Purity of each fraction was tested with anti-H3 antibodies by WB and protein quantified by Bradford assay. The cytosolic and nuclear fractions were stored at -80 ^{0}C until processed. For sphingolipid analysis 100 ml cytosolic or nuclear fraction were further diluted with 500 ml of methanol and spiked with deuterated sphingosines as internal standards. Lipids were extracted in a shaker for 1 h at 37°C. The mix was centrifuged at 15,000xg and supernatant transferred to a new tube. Lipids were hydrolyzed with 75 ml of methanolic HCL [1N HCL/10M water:methanol] and incubated for 16 h at 65°C. The acid was neutralized with 100 ml of ammonium hydroxide (2N) plus 500 ml water. The sample was vortexed, and the lower phase collected and dried under N_2 for analysis by MS.

Targeted metabolomics

Cell samples were collected and frozen at -80^{0}C until further use. For targeted metabolomic analysis, 400 mL of 2:2:1 mix of MeOH:ACN:H_2O was added to the cell pellets. The cell suspension was vortexed, placed in liquid N_2 for 1min, thawed, and sonicated for 15 min. This process was repeated twice. Samples were centrifuged to remove insoluble material and the supernatant was harvested and dried in Speedvac at 10°C. 100 mL of MeOH was added, samples were sonicated for 5 min on ice, centrifuged, and transferred to autosampler vials. The insoluble protein material was used to determine protein concentration by Bradford assay for sample normalization.

Amino acids

Samples were run on an Agilent 6495 QqQ with jet stream source coupled to an Agilent 1290 liquid chromatography stack with an Agilent HILIC-Z column, 2.1 x 100mm. The mobile phase was composed of A= 20mM ammonium formate, pH=3, and B= 90:10 ACN/H2O 20mM ammonium formate pH = 3. The gradient started at 100% B decreasing to 70% B in 12min and was held there for 3min (12 min – 15 min) before a 7 min post-run for column re-equilibration. The flowrate was set to 400 mL/min and the sample injection volume was 5 mL. Operating in positive ion mode, the source conditions were as follows: drying gas temperature set to 290 °C with a flowrate of 11 L/min, the sheath gas temp was 400 °C with a sheath gas flowrate of 11 L/min, the neb pressure set to 45 psi, cap voltage set to 2500V and nozzle voltage set to 0V. Data were processed using Agilent MassHunter Quantitative analysis software with calibration ranges of 2 to 100 mM prepared using authentic synthetic standards.

Sphingolipids

Samples were run on Waters Xevo TQ-S micro triple quadrupole mass spectrometer. The mobile phase was composed of phase A= 1mM ammonium formate/0.1% formic acid, and phase B= 90:10 IPA/ACN 1 mM ammonium formate/0.1% formic acid. The column used was a Waters Acquity UPLC BEH-C18 2.1x100 mm. The gradient started at 80% A, holding for 1.5 min then ramping to 97% B at T=18 min holding for 4 min. There was a 4 min re-equilibration step. The flowrate was set to 200 mL/min and the sample injection volume was 2 mL. Operating in positive ion mode, the source conditions were as follows: capillary voltage =1500 V, desolvation flow = 600 L/hr, desolvation temp = 350°C and cone flow = 50 L/hr. Data were processed using Waters TargetLynx software. For standard curves we used authentic synthetic standards and calibration levels ranges from 50 nM – 10,000 nM with the exception of 1-deoxysphingosine-14Z, which ranged from 5 nM – 350 nM.

Fatty acids

Samples were run on a Bruker Impact II Q-TOF coupled to an Agilent 1200 LC stack with an Agilent Zorbax 300SB-C18 column, 150 3 0.5 mm, mobile phase A = H2O/0.1% formic acid and mobile phase B = ACN/0.1% formic acid. The gradient started at 95% A, held there for 3 min, then ramped to 97% B at T= 21 holding for 4 min, followed by a 7 min re-equilibration step. The flowrate was set to 20 mL/min and the sample injection volume was 2 mL. Operating in negative ion mode, the source conditions were as follows: end plate offset = 500 V, capillary = 4,000 V, nebulizer pressure = 20 psi, drying gas flowrate = 7L/min at 180°C. Sample information was taken from Bruker Data analysis and entered into Microsoft Excel where a calibration curve was generated, and sample concentrations calculated.

Purification of bacterial NR2F1 and NR2F2 LBDs

Mouse NR2F1 LBD (NP_005645.1, aa 184-423) and NR2F2 LBD (NP_033827.2, aa 176-414) were amplified by PCR and cloned into a modified pET45b(+) vector containing a N-terminal 6xHis-GST tag which improved protein solubility. Plasmids were transformed into *E. coli* T7 Express competent bacteria (NEB). Bacterial cultures were grown at 37°C until the cultures reached an OD600 ~0.8. Protein expression was induced with 0.25-0.5 mM isopropyl-b-D-thiogalactopyranoside (IPTG)(American Bio) at 16°C for 18 h. Cells were harvested by centrifugation at 15,000xg and lysed by passing through the French express cell disruptor (1-2 cycles of 500 psi followed by 3-5 cycles of 1000 psi) in lysis buffer (50 mM Tris · HCl pH 8.0, 500 mM NaCl, 5% Glycerol, 1 mM EDTA, 0.5 mM TCEP (Sigma) plus protease inhibitor cocktail (Roche)). When 6xHis tag was used for purification, EDTA was omitted from the lysis buffer. Cell lysate was centrifuged at 20,000xg for 1 h and cleared supernatant was incubated with either Ni-NTA column (Qiagen) or Glutathione Sepharose-4B (GE Healthcare) pre-equilibrated with the lysis buffer. The 6xHis-tag purifications were extensively washed with wash buffer (20 mM Tris-HCl (pH 8.0), 500 mM NaCl, 20 mM imidazole, 5% glycerol with 0.5 mM TCEP) and eluted in same buffer with 200-500 mM imidazole. After washing with the lysis buffer, GST purifications were eluted with elution buffer (50 mM Tris · HCl pH 8.0, 250 mM NaCl, 10 mM reduced Glutathione (Sigma)). The eluate was pooled, concentrated, and further purified by SEC650 column on FPLC (Bio-Rad) in FPLC buffer (20 mM Tris$HCl pH 8.0, 250 mM NaCl) to produce the monomeric form of the receptor.

Purification of mammalian NR2F2 LBDs

We removed the first 22 amino acids and last 10 amino acids of NR2F2-LBD to increase protein stability. The truncated LBD was fused to a N-terminal His-tag and cloned into the pcDNA3.1 vector. A factor Xa site was introduced to allow for cleavage of the His-tag. Protein was produced by transfecting suspension HEK293-FT cultures growing in FreeStlye F17 expression medium (Thermo Fisher). Transfections were performed with 200 mg of plasmid DNA complexed with PEI (0.5 mg DNA/1.5 mg PEI) prepared in FreeStlye F17 expression medium.

Fluorescence polarization assay (FPA)

Fluorescein labelled co-activator and co-repressor peptides FL-SMRT-ID2, FL-SMRT-ID1, FL-PGC1A, FL-SRC2-1, FL-SRC2-2 and FL-SRC2-3 (Life Technologies) were first tested for specificity by incubating 5 nM of each peptide with 100 nM of the apo (empty) receptor LBDs of NR2F1/NR2F2/NR2F6 plus 5 mM vehicle to test whether peptide can bind to empty receptor. Next, we tested whether unrelated compounds could promote non-specific peptide binding by adding 5 mM vehicle, D-erythro-sphingosine, 7-dehydrocholesterol or 10-Nitrooleic acid. In these tests, SRC2-2 was determined to have the lowest background on Apo receptor or receptor incubated with unrelated compounds. Thus, the fluorescein conjugated SRC2-2 peptide was used in all FPA assays presented in the manuscript. FPAs were performed by incubating 5 nM of fluorescein-labeled SRC2-2 peptide with purified NR2F1 or NR2F2 LBDs in its apo-form or saturated by each individual compound for 1 h at room temperature. The proteins were assayed as serial dilutions in the binding buffer (20 mM Tris-HCl (pH 8.0), 200 mM NaCl, 10 mM DTT), the metabolites were used at 5 mM of concentration. The FPA measurements were carried out in triplicates using black 96-well plates or 384 well plates (Thermo Fisher). FPA signals were measured on the Spectramax M5 reader (Molecular Devices). The data processing and the Kd value calculations were performed using GraphPad Prism 5 (Graphpad).

Thermal shift assays using recombinant NR2F2-LBD

Thermal shift assays were performed using SYPRO fluorescent dye (Lo et al., 2004). 6xHis-tagged NR2F2-LBD was produced by overexpression in HEK293 cells and purified with a Nickel NTA chromatography column as described above. SYPRO Orange (Thermo Fisher) was diluted in H_2O, from 5,000x commercial stock to 50x working stock. 12.5 mM working stock of NR2F2-LBD was prepared in elution buffer (50 mM Tris pH 8.5, 500 mM NaCl, 5% glycerol). The following metabolites were tested: 1-deox- ySO-14Z, D-erythro-sphingosine, Sphinga-4,14-diene, 1-desoxymSA and vehicle. The metabolites were prepared as a 125 mM working stock in ethanol. Reaction mixture was as follows: 10mL protein (5 mM final concentration), 1mL metabolite (5 mM final concentration), and 11.5 mL elution buffer. The reaction mixture without SYPRO was incubated at 4°C for 30 min to allow for metabolite binding. After incubation, 2.5 mL of 50x SYPRO Orange stock was added to the reaction mixture to obtain final reaction concentration of 5X SYPRO Orange. Reaction mixtures were loaded, in sextuplicate, into Bio-Rad 96-well qPCR plates. Melting curves were generated using the Bio-Rad CFX Real-Time PCR system according the manufacturer's instructions.

Surface plasmon resonance (SPR)

SPR was measured using the T100 system (Biacore). Recombinant 6xHis-tagged NR2F2-LBD was produced in mammalian cells as described above. The protein was non-covalently bound to the nickel NTA sensor chip (Series S) (GE Healthcare Life Sciences) with an RU of 1,000 using the running buffer HBS-P+ (10 mM Hepes pH 7.4, 150 mM NaCl, 0.05% surfactant P20) (Fisher Scientific). For metabolite capture and regeneration, we used HBS-P+ as running buffer and the following program: surface activation 0.5 mM $NiCl_2$ with a flow rate of 10 mL/min, contact time 90 sec and washing time 60 sec. Protein was captured from 20 mg/mL solution at a flow rate of 10 m L/min for 500 sec. After metabolite binding, the chip was regenerated twice, once with 350 mM EDTA with a flow rate of 30 mL/min, contact time 60 sec and washing time 60 sec, and a second regeneration with 10 mM Glycine pH2.5 in HBS-P+ buffer with a flow rate of 30 mL/min, contact time 60 sec and washing time 60 sec. For binding assessment, measurements were run using the HBS-P+ buffer with a flow rate of 30 mL/min, association time 180 sec, dissociation time 600 sec and stabilization time of 10 sec. Metabolites were prepared in HBS-P+ buffer as serial dilutions of 800 nM, 600 nM, 400 nM, 200 nM, 100 nM, 50 nM and 0 nM. The 0 nM concentration was used to define the blank for background subtraction of the sensorgrams. Each dilution was run and then the two regeneration cycles performed before the next dilution was tested. Three metabolites were tested: sphinga-4,14-dienine, 1-deoxySO and D-erythroSO.

Conditional deletion of *Sptlc2* and *Nr2f2* in mice

Sptlc2$^{f/f}$ and Nr2f2$^{f/f}$ mice were crossed with Cdh5^{CerERT2} or Prox1^{CreERT2} mice to obtain Sptlc2$^{f/+}$Cdh5$^{CerERT2/+}$, Nr2f2$^{f/+}$Cdh5$^{CerERT2/+}$, Sptlc2$^{f/+}$Prox1$^{CerERT2/+}$and Nr2f2$^{f/+}$Prox1$^{CerERT2/+}$ animals. For genotyping of young animals, genomic DNA was extracted from the ears or tails. Embryo genotyping was performed using extraembryonic tissues (placenta, amnion) or embryonic tails. DNA extractions were performed using the HotStart mouse genotyping kit (Kapa Biosystems) and PCR were performed using the GoTaq green master mix (Promega) using the primers listed in Table S1, Primers-Mouse Genotyping. The PCR conditions were as follows. For Sptlc2-Flox: 94°C 5 min, 30 cycles of 94°C for 1 min, 59°C for 1 min and 72°C for 1 min, followed by 72°C for 5 min. Wild type allele produced a 420 bp product, Sptlc2-loxP allele produced a 600 bp product. For Nr2f2-Flox we used primers designed by (Takamoto et al., 2005): 95°C 8 min, 35 cycles of 95°C for 15 sec, 56°C for 30 sec, 72°C for 1 min followed by 72°C for 5 min. Wild type allele produced a 785 bp product, Nr2f2-loxP allele produced a 394 bp product. For Prox1-CreERT2: 95°C for 2 min, 35 cycles 95°C for 15 sec, 60°C for 30 sec, 72°C for 1 min followed by 72°C for 2 min. The Prox1-CreERT2 transgene produced a 730 bp product. For Cdh5-CreERT2:

95°C for 3 min, 35 cycles of 95°C for 15 sec, 60ºC for 15 sec, 72°C for 15 sec followed by 72°C for 5 min. Cdh5-CreERT2 transgene produced a 548 bp product. PCR products were resolved in 1% agarose gel.

Deletion efficiency after tamoxifen injection

The efficiency of deletion after tamoxifen injection was estimated using hearts and tails of E15.5 embryos or sorted Prox1+ cells. To obtain Prox1+ cells, embryos were homogenized and digested in tissue digestion buffer (1%FCS in DMEM, 0.5mg/mL Collagenase D (Sigma), 40mg/mL DNase I(Sigma)) for 1 h in a shaker at 90 rpm at 37°C. The digested cells were filtered through a 100 mm cell strainer (Fisher Schientific) and centrifuged at 700xg for 5 min. The cells were fixed using fixation/permeabilization solution (Thermo Fisher) according to the manufacturer's instructions. Fixed and permeabilized cells were incubated with anti-mouse CD16/CD32 (Bio Cell) at 4°C for 15 min in the dark, then incubated for 1 h with AF405 labelled anti-mouse Prox1 antibody (Novus Biologicals) at 4°C for 1 hour in the dark. Cells were washed, resuspended and Prox1 positive cells were sorted using the BD Aria II sorter. DNA was extracted as described above. Quantitation was performed by PCR using two sets of primers listed in Table S1, Primers-PCR deletion efficiency. Set 1 amplifies a fragment of 199 bp in the floxed region of *Sptlc2* deleted by Cre recombinase and Set 2 amplifies a 200 bp region in the non-deleted exon2 of the *Sptlc2* gene. Control primer set was used to normalize DNA quantities across the samples. PCR products were resolved in 1% agarose gels and imaged. Band intensities were obtained with ImageJ and normalized to the intensity of the control PCR products.

Embryo processing, staining, and imaging

For time mated pregnancies, mating of 6-12 weeks old *Sptlc2*$^{f/f}$*Prox1*^{CreERT2} *or Sptlc2*$^{f/f}$*Cdh5-CreERT2* males and *Sptlc2*$^{f/f}$ or *Sptlc2*$^{f/+}$ females was performed as follows. Embryonic day 0 was defined as the day males and females were placed together. At day 10, pregnant females were injected with 100 mL of 10 mg/mL of Tamoxifen (Sigma) dissolved in Sunflower seed oil (Sigma). Embryos were collected at days E13.5 and E15.5, washed twice in ice cold PBS pH7.5 and photographed before further processing. The embryos were placed in fixative containing 0.4% paraformaldehyde (PFA) (Electron Microscopy Sciences) in Ca^{++} $MgCl_2^{++}$ containing DPBS (Gibco). The embryos were fixed overnight at 4°C on a rocking platform. Next day the embryos were transferred to Ca^{++} $MgCl_2^{++}$ containing DPBS with 0.1% NaN3 and stored at 4°C until use. For light sheet microscopy, the embryos were stained using the iDisco protocol (Renier et al., 2014). Embryos were dehydrated in methanol and incubated overnight in 5% H_2O_2 in methanol at 4°C, rehydrated and permeabilized at 37°C in DPBS, 0.3 M Glycine, 0.2% TX-100 and 20% DMSO for maximum 2 days. After blocking in 5% donkey serum, the embryos were incubated with primary antibodies for 4 days (E13.5) or 5 days (E15.5) at 37°C. After washing, embryos were incubated with secondary antibodies following primary antibody incubation protocol. Finally, the embryos were dehydrated and cleared in methanol and benzyl benzoate. The Ultramicroscope II (Lavision Biotec) was used for the image acquisition. Images were processed using the Imaris v9 software (Bitplane Technologies) for data analysis and 3D rendering. The lymphatic surface area was measured in Imaris by applying the surface area tool. To stain the lymphatic endothelial cells, we used anti-Lyve1 (Reliatech) and anti-Prox1 (R&D technologies). Blood vessels and lymphatic vessels were visualized with anti- CD31 (Thermo Fisher). Secondary antibodies were donkey anti-rabbit Alexa 555 (Thermo Fisher), donkey anti-rat Alexa 790 (Jackson Immunoresearch), and donkey anti-goat Alexa 647 (Thermo Fisher).

Rescue experiments using mouse lymphatic endothelium

Lymphatic endothelial cells (LECs) were isolated from mouse lymph nodes digested with Collagenase D (Sigma) and Dispase (Stem Cell Technologies). LECs were cultured as previously described (Jordan-Williams and Ruddell, 2014). For LECs grown in semi-synthetic medium, LECs were plated on Lab-TEK II chamber slides (Nunc) and cultured overnight in semi-synthetic medium (SSM) containing DMEM, 10 mM Hepes, 1%BSA, and 1 mM D-erythroSO-BSA complexes, 1x Insulin-Transferrin-Selenium (ITS-A) (Thermo Fisher), 10 mM b-mercaptoethanol, 0.2 mM Glutamine and 1% FBS. 0.5-1 mM of 4-hydroxytamoxifen (4-OH-TMX) (Sigma) were added to induce deletion of *Nr2f2* or *Sptlc2*. The D-erythroSO was added to all samples to replenish the precursor required for synthesis of membrane sphingolipids and is essential for cell survival (Hanada et al., 1992). The 4-OH-TMX-treated cells were divided into three groups: plus or minus desired concentration of 1-deoxySO (14Z)-BSA complexes and vehicle. In LECs grown in SSM the concentrations of 1-deoxySO-14Z used was 50-100 nM. Cells that did not receive 4-OH-TMX were used as controls. All groups of cells received fresh media and appropriate metabolites daily for continued culture. Cells were processed for immunostaining 24 h after the 4-OH-TMX administration as follows. Cells were fixed with 4% paraformaldehyde (Electron Microscopy Sciences), washed 3 times with PBS supplemented with 0.3% Triton X-100 (PBST), blocked for 2 h with PBST containing 5% goat serum and stained overnight with anti-NR2F2 antibody (Abcam). Cells were washed 3 times with PBST, stained for 1 h with goat anti-mouse-Alexa 488 antibody (Thermo Fisher) and washed 3 times with PBST. Cells were then blocked for 30 min with PBST containing 5% goat serum and stained for 1 h with anti-mouse Prox1antibody conjugated to Alexa 405 or Alexa 647 as indicated (Novus Biologicals) and anti-mouse MECA-79 Alexa 488 (Thermo Fisher). Cells were washed 3 times with PBST, mounted and imaged using the Leica S5 confocal microscope. Images were analyzed and processed using Leica LAS X software. For flow cytometry, LECs were grown in 12-well tissue culture plates using vascular cell basal medium (ATCC) containing 2.5% FBS supplemented with endothelial cell growth kit-VEGF (ATCC) and 1 mM D-erythroSO-BSA complexes. Control samples received 1.25 mM vehicle (ethanol)-BSA conjugate, experimental group 1 samples received 1.25 mM vehicle-BSA conjugate plus 5 mM 4-OH-TMX while experimental group 2 received 1.25 mM 1-deoxySO-14Z-BSA conjugate plus 5 mM 4-hydroxytamoxifen 4-OH-TMX. After 48 h of culture, single cell suspensions were obtained using TrypLE (Thermo Fisher), cells were washed once in PBS, fixed and analyzed on Cytoflex flow cytometer (Beckman Coulter). Data analyses were performed using FlowJo version 10 software.

Rescue experiments using ex-vivo embryo culture

E10.5 *Sptlc2*$^{f/f}$ *Cdh5*$^{CreERT2/+}$ embryos were harvested, washed once with pre-warmed PBS, placed in DMEM-F12 media (Thermo Fisher) supplemented with 5% FBS and equilibrated in 37°C incubator with 5% CO_2. The extra-embryonic tissues were removed using a dissection microscope. Embryos were divided in two groups. The experimental group was cultured in embryo culture medium containing DMEM-F12 (Thermo Fisher), 15% KSR (Thermo Fisher), 1x N2 supplement (Thermo Fisher), 1x Glutamax (Thermo Fisher), 2.5 mL/mL of 100x Pen-Strep solution (Thermo Fisher), 1 mM 4-OH-TMX (Sigma), 5 mM D-erythroSO-BSA complexes and 25 nM 1-deoxySO-BSA complexes. Control group embryos were cultured similarly but received vehicle-BSA complexes in place of 1-deoxySO-BSA complexes. Cultures were carried out in 50 mL conical tubes in high O_2 atmosphere which was created by attaching a Steriflip filter unit (Millipore Sigma) connected to an O_2 tank for 20-30 sec. The tubes were sealed with parafilm and placed in roller bottle in a 37°C incubator with 5% CO_2 for 24 h. The embryos were then washed in PBS with Ca^{+2} and Mg^{+2} (Thermo Fisher) and fixed overnight in $Ca^{+2}Mg^{+2}$ PBS plus 0.4% PFA (Electron Microscopy Sciences 15710). The fixed embryos were washed with PBS and stored in PBS plus 0.1% Sodium Azide. Embryos were genotyped and processed for light sheet microscopy as described above.

Generation of *NR2F2*-KO and *NR2F1/2*-dKO hESC lines

CRISPR/Cas9 editing of *NR2F2* gene was performed with two gRNAs targeting exon 2 that are predicted to delete ~300 bp region of the gene (Table S1 – gRNAs). gRNAs were purchased as custom-made oligonucleotides (Eurofins Genomics), annealed and cloned into the LentiCRISPR V2 vector (Sanjana et al., 2014; Shalem et al., 2014). H9 hESCs were treated with Accutase (Stem Cell Technologies), washed and resuspended in 800 mL cold PBS, and mixed with 40 mg of each gRNA. Cells were electroporated using Gene Pulser XcelI (Bio-Rad) at 250 V, 500 mF in a 0.4 cm Gene Pulser cuvette (Bio-Rad). Cells were plated onto a Matrigel (Corning)-coated tissue culture dish in mTeSR1 media (Stem Cell Technologies) supplemented with 5 mM ROCK inhibitor Y27632 (Tocris) for the first 24 h. Two days after electroporation, Puromycin (Sigma) was added at 1 mg/mL concentration for 48 h. Individual colonies were picked and expanded in 6-well plates. Genomic DNA was purified using the KAPA Express Extract Kit (Kapa Biosystem). Deletions were validated by PCR using primers listed in Table S1-PCR primers for deletion screen. The PCR products were sequenced to confirm sequences of each *NR2F2* allele using the Table S1-sequencing primers. The absence of protein in the KO clones was confirmed by Western blotting of day 7 cardiomyocyte lysates. To generate *NR2F1/2*-DKO hESCs, two *NR2F2*-KO clones were electroporated with a mixture of *NR2F1* gRNAs. Clone selection and validation was as described above for a single *NR2F2* knockout. Two independent DKO clones showed similar behavior in the differentiation protocol.

Generation of Dox-inducible *SPTLC1*^{C133W} (*HSAN*) hESC lines

The targeted knockin of the *SPTLC1*^{C133W} and rtTA transgenes into the AAVS1 locus was performed as previously described (Wang et al., 2018; Wang et al., 2019). WT or DKO hESCs were treated with Accutase, washed and 2-3 x 10^6 cells resuspended in 100 mL cold R buffer from the Neon transfection system kit (Thermo Fisher) and mixed with plasmid mix consisting of 2.5 mg AAVS1-TALEN-L, 2.5mg AAVS1-TALEN-R, 10 mg Puro-FLAG- *SPTLC1*^{C133W} donor and 10 mg Neo-M2rtTA donor. Cells were electroporated using the Neon Transfection System (Invitrogen) at 1050 V 2x30 millisecond pulses and plated on Matrigel-coated tissue culture plates in StemFlex™ medium (Thermo Fisher), supplemented with 5 mM ROCK inhibitor for the first 24 h. Two days after electroporation, cells were selected with 50 mg/mL Geneticin (Life Technologies) for 4 days, followed by treatment with 0.5 mg/mL Puromycin (Life Technologies) for another 2 days. Individual colonies were picked and expanded in StemFlex™ medium. Integration into the AAVS1 locus was confirmed by PCR. Dox dependent transgene expression was validated by Western blotting with anti-FLAG antibody.

Cardiomyocyte differentiation of hESCs

Cardiomyocyte differentiation was performed as described in (Burridge et al., 2014; Lian et al., 2013) with minor modifications. Prior to differentiation, hESCs were cultured in E8 medium. Single cells were prepared using Accutase and plated onto Matrigel-coated 12-well tissue culture plates in E8 medium supplemented with 5 mM ROCK inhibitor for the first 24 h. Plating densities were adjusted to obtain 75–85% confluent wells at day 4 after plating. This time point was considered a day 0 of differentiation protocol. To initiate differentiation, cells were cultured in RPMI-1640 medium (Gibco) supplemented with Insulin-free B-27 (Thermo Fisher) and 6 mM CHIR99021 (Tocris) for 48 h followed by a 24-hour culture in Insulin-free RPMI/B27 medium without inhibitor. 72 h after addition of CHIR99021, cells were switched into the Insulin-free RPMI/B27 supplemented with 5 mM IWP2 (Tocris). On day 5 of differentiation, the media was replaced for the Insulin-free RPMI/B27 medium without inhibitor. On day 7 of differentiation and every two days there- after, media was replaced for fresh Insulin-containing RPMI/B27 medium.

Myriocin treatments were initiated on day1 and included a vehicle (DMSO) control and 1 mM Myriocin (Sigma).

D-erythroSO-BSA and 1-deoxySO-BSA complexes were added at 1.5 mM concentration on day 3 of differentiation and every two days thereafter. Expression of *SPTLC1*^{C133W} (*HSAN*) mutant in WT^{HSAN} and DKO^{HSAN} hESC lines was induced by adding 2 mg/mL Doxycycline (Sigma) on day 3 and every two days thereafter.

TNNT2 staining of cardiomyocytes

Cardiomyocyte cultures were treated with Accutase (Stem Cell Technologies) to obtain single cell suspension. Cells were pelleted, washed once in PBS and then fixed and permeabilized using the BD Cytofix/Cytoperm fixation/permeabilization kit (BD Biosciences). The cells were stained with anti-cardiac troponin T Alexa 647 antibody (BD biosciences) for 30 min, washed once in PBS and

resuspended in PBS at a density of $1x10^6$ cells/mL. Data were collected on the CytoFlex instrument (Beckman Coulter) and analyzed in FlowJo v.10.

Electron microscopy of hESC-derived cardiomyocytes

Day 12 cardiomyocyte cultures were fixed in 0.1 M sodium cacodylate buffer (pH 7.4) containing 2.5% glutaraldehyde for 1 h at room temperature. After cells were rinsed in the same buffer twice, they were post-fixed in 1% OsO_4 at room temperature for 1 h. Specimens were stained en bloc with 2% aqueous uranyl acetate for 30 min, dehydrated in a graded series of ethanol to 100% and embedded in EMbed 812 resin. Blocks were polymerized at 60°C overnight. Thin 60 nm sections were cut using a Leica ultramicrotome and post-stained with 2% uranyl acetate and lead citrate. Cell sections were examined with a FEI Tecnai transmission electron microscope at 80 kV accelerating voltage; digital images were recorded with an Olympus Morada CCD camera and iTEM imaging software.

RNA isolation

Total RNA was isolated using Trizol Reagent (Thermo Fisher), treated with DNAse I (Ambion) to remove genomic DNA, precipitated, washed with 70% ethanol and dissolved in water.

Reverse Transcription and quantitative PCR (RT-qPCR)

1 mg of total RNA was reverse transcribed using random hexamers and SuperScript II Reverse Transcriptase (Invitrogen). Resultant cDNA was diluted in water and 20 ng was used in each RT-qPCR reaction. Reactions were run on a CFX96 instrument using iTaq Universal SYBR Green Supermix (Bio-Rad). Standard curves were generated for each primer set and were used to calculate Ct values with the expression threshold set to 100 RFU. In order to compare expression levels between different samples, all expression values were scaled to GAPDH. The gene-specific primers used in PCR-based analyses, included those published previously (Osafune et al., 2008; Wang et al., 2012)are listed in Table S1-qPCR Primers.

Immunoblotting

Cells were washed twice in ice-cold PBS and incubated in 1X RIPA buffer (Thermo Fisher) with 1X PhosSTOP protease inhibitor(Roche) and 1X cOmplete Protease Inhibitor Cocktail (Roche) for 5 min on ice. Lysates were pre-cleared by maximum speed centrifugation in a benchtop centrifuge for 30 min and protein was quantified using the Bio-Rad Protein Assay Kit II (Bio-rad). 20 mg of protein lysate was resolved on SDS-PAGE gel and transferred onto an Immobilon membrane (Millipore). Blots were blocked in 5% non-fat dry milk, incubated with primary antibody overnight at 4°C, washed, incubated with secondary antibody for 1 h at room temperature, washed, and developed with SuperSignal West Pico Chemiluminescent Substrate (Thermo Fisher). TUBULIN, GAPDH or histone H3 were used as loading controls. A complete list of antibodies used in this study is listed in Table S1-Antibodies.

Basic statistical analyses

Statistical analyses were performed using GraphPad Prism 5 and Excel software. Unless otherwise stated, data are shown as averages with standard deviations. Exclusion of samples with at least ±2 sd from the mean was only performed in statistical procedures that require two independent samples of equal size. Whenever possible, experiments were designed so that samples under comparison are of equal sizes. Basic comparisons were performed using non-randomized data analyzed by two-tailed Student's t test either paired or unpaired using equal or unequal variance as indicated.

Bulk RNA-seq analyses

RNA samples were processed by the Yale Center for Genome Analyses according to standard Illumina protocols. Libraries were sequenced on the NovaSeq flow cell with 100 bp paired-end reads. Signal intensities were converted to individual base calls during the run using the system's Real Time Analysis (RTA) software. Base calls were transferred from the machine's dedicated personal computer to the Yale High Performance Computing cluster via a 1 Gigabit network mount for downstream analysis. Sample de-multiplexing and alignment to the human genome - was performed using Illumina's CASAVA 1.8.2 software suite.

Untrimmed FASTA files were mapped with Salmon (version 0.8.2) using GENECODE version 38 (GRCh38.p12) reference transcriptome. DeSeq2 package was used to determine differential expression between samples. Data were processed on the Galaxy server (https://usegalaxy.org/).

Genes with expression fold changes greater than 2 and p values less than 0.05 were considered differentially expressed. Additional filtering was applied to remove genes with expression levels below 5 TPM in all samples. Gene ontologies were defined using Panther (www.pantherdb.org/) and NIH David (https://david.ncifcrf.gov/) packages. List of NR2F2 target genes identified by ChIP was obtained from (Churko et al., 2018; Wu et al., 2013).

Single-cell (sc)RNAseq of cardiomyocyte differentiation and data analyses

Live cells from WT, NR2F2-KO and NR2F1/2-DKO cultures were sorted and analyzed in duplicates on day 6 and 19 of cardiomyocyte differentiation. Single cell separation, library preparation, and sequencing were performed by the Yale Center for Genome Analyses according to standard 10x Genomics protocols. Minimum sequencing depth was 20,000 read pairs per cell. Cell Ranger™ analysis pipeline was used for initial analysis and visualization.

Data from all 6 samples for each time point (Day 6 and Day 19) were concatenated into a single matrix for analysis. The number of cells in each sample were as follows: WT-R1– 11,506 cells, WT-R2 – 9,836 cells, KO-R1– 9,272 cells, KO-R2–19,454 cells, DKO-R1–12,658 cells, DKO-R2 –21277 cells for day 6, and WT-R1–8,821 cells, WT-R2 –13,424 cells, KO-R1–16,214 cells, KO-R2–19,422 cells, DKO-R1–37,637 cells, DKO-R2–33,183 cells for day 19. For data pre-processing, we followed the current best practices in single-cell RNA sequencing analysis based on the SCANPY toolkit (Luecken and Theis, 2019; Wolf et al., 2018). Genes detected in less than 50 cells were removed. Cells with mitochondrial read percentages larger than 20% were removed. Cells with the total UMI count larger than 50,000 for Day 6 and 25,000 for Day 19 were removed. All filtering decisions were made by manual inspection of the data distributions using SCANPY. The filtered data contained 73,202 cells/19,008 genes at day 6 and 119,758 cells/19,134 genes at day 19. The filtered data were then library-size normalized and square-root transformed using scprep (www.github.com/KrishnaswamyLab/scprep), as previously described (Burkhardt et al., 2019; Moon et al., 2019). To build a cell similarity graph, 100 PCA dimensions were calculated and edge weights between cells were calculated using an alpha-decay kernel as implemented in the graphtools library (www.github.com/KrishnaswamyLab/graphtools) using knn=9 and decay=10. This graph was then used for the MELD analysis (Burkhardt et al., 2019) to calculate the enhanced experimental signal (EES) for each sample with default parameters. The graph was also used for PHATE embedding (Moon et al., 2019) visualization using default parameters. For clustering, we used k-means clustering with k = 30 and the PHATE diffusion potential (Moon et al., 2019). Analysis of groups of genes was done by the scoring method, ‘‘scanpy.tl.score_genes’’, in SCANPY. Identification of marker genes for each cluster were done by the ranking method, ‘‘scanpy.tl.rank_genes_groups’’, with logistic regression in SCANPY.